— Review —

Recent Progress in Electrochemical Surface Science with Atomic and Molecular Levels

Shen YE,[a,b] Toshihiro KONDO,[c] Nagahiro HOSHI,[d] Junji INUKAI,[e] Soichiro YOSHIMOTO,[f] Masatoshi OSAWA,[a] and Kingo ITAYA[g,h]

[a]Catalysis Research Center, Hokkaido University (N21 W10, Kita-ku, Sapporo 001-0021, Japan)
[b]PRESTO, Japan Science and Technology Agency (JST).
[c]Graduate School of Humanities and Sciences, Ochanomizu University (2-1-1 Ohtsuka, Bunkyo-ku, Tokyo 112-8610, Japan)
[d]Department of Applied Chemistry and Biotechnology, Graduate School of Engineering, Chiba University (1-33 Yayoi-cho, Inage-ku, Chiba 263-8522, Japan)
[e]Fuel Cell Nanomaterials Center, University of Yamanashi (4 Takeda, Kofu 400-8510, Japan)
[f]Priority Organization for Innovation and Excellence, Kumamoto University (2-39-1 Kurokami, Kumamoto 860-8555, Japan)
[g]WPI Advanced Institute for Material Research, Tohoku University (6-6-07 Aoba, Sendai 980-8579, Japan)
[h]Department of Applied Chemistry, Graduate School of Engineering, Tohoku University (6-6-07 Aoba, Sendai 980-8579, Japan)

Received October 9, 2008 ; Accepted December 12, 2008

Until the mid 1980's, there had been only few *in situ* methods available for structural determination of an electrode surface in solution at atomic and monolayer levels. Nowadays, many powerful *in situ* techniques, such as electrochemical scanning tunneling microscopy (EC-STM), infrared reflection absorption spectroscopy (IRAS), surface-enhanced Raman scattering (SERS), and surface-enhanced infrared reflection absorption spectroscopy (SEIRAS), second harmonic generation (SHG), sum frequency generation (SFG), and surface X-ray scattering (SXS) have been widely employed to characterize the electrode surfaces under potential control with atomic and/or molecular resolution. The object of this review is to highlight some of the progress on *in situ* methods at solid-liquid interface with atomic and molecular levels. Several selected topics are focused on, specifically adsorbed anions on metal surface, electrocatalysis of the carbon oxide oxidation and oxygen reduction, and direct observation of single crystal electrode surfaces.

Key Words : Solid-Liquid Interface, Single Crystal Electrode, Adsorption, Structure, Adlayer, Electrocatalysis, SHG, SFG, SXS, SEIRAS, STM

1 General Introduction

Kingo ITAYA & Soichiro YOSHIMOTO

Electrochemistry is important for industries concerned with products and processes such as batteries, fuel cells, electroplating, corrosion inhibition, electro-organic synthesis, and sensor devices.[1] Because electrode reactions take place at solid-liquid interface where the electrode is in contact with a solution, electrochemical interface plays an important role in controlling the electron transfer reaction. Understanding the nature of solid-liquid interface in detail not only leads to the elucidation of the electrode reaction mechanism but also provides information useful for designing new interfaces.

As a fundamental basis for all electrochemical studies, electrode-electrolyte interfaces must be prepared reproducibly, and methods must be established to observe these interfaces accurately. It is still difficult to elucidate electrochemical reactions on the atomic scale using polycrystalline electrodes. Well-defined single crystal surfaces must be exposed to solution to understand surface structure-reactivity relationships on the atomic scale. Efforts have succeeded to produce extremely well-defined, atomically-flat surfaces of various electrodes made of noble metals, base metals, and semiconductors without either oxidation or contamination in solution.[2-4]

It was first realized in 1980 in the field of *electrochemical surface science* that the adsorption-desorption reaction of hydrogen on Pt single crystal electrodes is strongly dependent on their crystallographic orientations; this demonstrated the importance of the nature of metal surface at the atomic level.[5,6] Clavilier was the first to develop a simple and important experimental method, the so-called *flame annealing and quenching method*,[5] to expose well-defined electrode surfaces in aqueous electrolyte solutions without the use of ultrahigh vacuum (UHV) techniques. Nowadays, this technique has been extended by Hamelin for Au,[7,8] by Motoo and Furuya for Ir,[9] and by Itaya's group for Rh and Pd.[10]

Meanwhile, since the late 1980's, *in situ* analytical methods were developed all over the world. In the early stage, various experimental techniques, such as infrared absorption spectroscopy (IRAS),[11,12] ultra-violet (UV)-visi-

ble reflectance spectroscopy, and low-energy electron diffraction (LEED) in UHV have been applied to understand the electrode-electrolyte interface.[13,14] In particular, electrochemical scanning tunneling microscopy (EC-STM) is now widely accepted as one of the powerful tools for generating the understanding of the structure of adsorbed layers of molecules on metal surfaces at the atomic scale in solution[15-20] as well as in UHV.[21,22] It cannot be overemphasized that *in situ* STM and AFM allowed us not only to determine the surface structure, but also to follow various electrochemical reactions, such as the deposition and dissolution of atoms and molecules.[3,17,19]

Subsequently, quartz crystal microbalance (QCM),[23-28] and surface-enhanced Raman scattering (SERS),[29] surface-enhanced infrared reflection absorption spectroscopy (SEIRAS),[30-32] second harmonic generation (SHG),[33-36] sum frequency generation (SFG),[37-44] and surface X-ray scattering (SXS)[45-47] methods were developed for surface structural investigations of electrochemical processes taking place at electrode-electrolyte interfaces with a monolayer level, by the combination of electrochemistry.[4] Thus, the establishment of both the preparation of well-defined electrode surfaces and *in situ* characterization techniques make it possible to monitor with atomic and/or molecular levels for *not only* electrode processes including underpotential deposition (UPD) of metal ions[3,18,48] and specifically-adsorbed anions,[3,17,18] ***but also*** formation and characterization of self-assembled monolayers (SAMs) of organothiols[49-52] and supramolecularly-organized molecular adlayers through hydrogen bonding formation,[53-55] donor-acceptor interaction,[55-58] and electrostatic interaction.[59]

One of the goals of interfacial electrochemistry is to control electrochemical reactions precisely with atomic and molecular scales.[3,19,60-62] It is reasonably expected that the precise control of electrochemical reactions can produce many ultra-fine and nanomaterials at atomic and molecular scales.[63-65]

In this review, a recent advance in *in situ* electroanalytical methods such as SXS, IR, SHG, SFG, and STM combined with single crystal electrochemistry is reported from the members of nano-interface division in ECSJ. Details are described in respective section below.

2 SXS for Gold Single-crystal Electrodes

Toshihiro KONDO

The structure of the surfaces can be investigated with SXS within the surface plane and along the surface normal by controlling the direction of the scattering vector Q, which is the difference between the incident and scattered X-ray wave vectors.[66,67] Information within the surface plane is typically obtained by orienting Q almost within the surface plane. This corresponds to the grazing incidence angle geometry where the angle is typically a few degrees. The measurement in this geometry is so-called the in-plane measurement and this method is so-called surface X-ray diffraction (SXRD), which is one of the SXS methods. On the other hand, when Q is aligned entirely along the surface normal direction, information about the surface normal structure is obtained. This geometry is referred to as specular reflectivity since the angle between the surface plane and incident wave vector is equal to the angle between the surface plane and the scattered wave vector. Additional structural information can be obtained by determining the scattered intensity distribution along the surface normal direction at a fixed, finite in-plane wave vectors corresponding either to the bulk crystal structure or to the overlayer structure. Such scattered intensity distribution along the surface normal is so-called crystal truncation rod (CTR) and then this method is so-called CTR technique, which is also one of the SXS methods. Thus, the combination of these methods, i.e., SXRD and CTR, allows us to obtain the three-dimensional (3D) structure with an atomic dimension and therefore, SXS technique is one of the best methods to investigate the 3D interfacial structure at electrochemical interfaces *in situ*.[66-71]

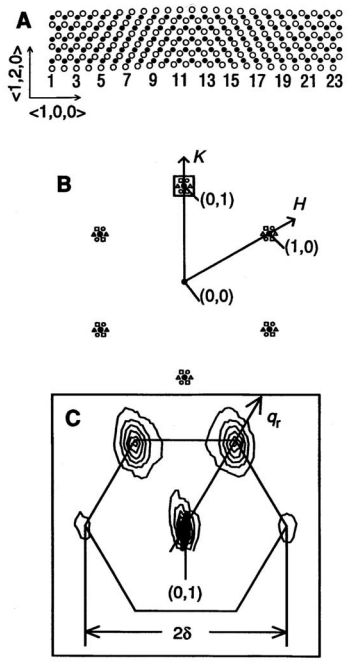

Fig. 1 (A) In-plane hexagonal structure of the Au(111) surface. The solid (open) circles correspond to atoms in the second (first) layer. Surface atoms in the left and right sides of the figure are in undistorted hexagonal sites, whereas in the center of the figure the atoms are in faulted sites. For 24 surface atoms in place of 23 underlying surface atoms along the $<1,0,0>$ direction, the compression is $24/23 - 1 = 4.4\%$ and $\delta = \sqrt{(3/2)}/23 = 0.038$. (B) In-plane diffraction pattern from the Au(111) surface. Solid circles represent diffraction from the underlying hexagonal lattice. Open symbols originate from the $(23 \times \sqrt{3})$ reconstructed phase with three rotational equivalent domains (circles, squares, and triangles). The axis, q_r, is defined to be along the (1,1) direction. (C) Equal-intensity scattering contours in the vicinity of the (0,1) reflection at L = 0.5 measured in 0.01 M NaCl at –0.3 V. Reprinted with permission from Ref. 45, Copyright American Physical Society (1992).

Many *in situ* structural studies at single-crystal electrode/electrolyte interfaces using the SXS technique have been carried out in the last 15 years.[45,46,71-85] In this section, we focus on the gold single-crystal electrodes because gold is one of the most popular electrode materials and the structures of the gold single-crystal electrode surfaces at various potentials using *in situ* SXS technique including our results will be reviewed.

As far as the structure of gold electrodes is concerned, Ocko *et al.* investigated for the first time the structures of the reconstructed Au(111),[45,46,71,72] Au(100),[73] and Au(110)[74] surfaces using *in situ* SXS. Especially, the reconstruction formation/lifting transition of the Au(111) surface was investigated in details in the electrolyte solutions containing various halogen anions.[45,46,71,72]

Despite the underlying hexagonal symmetry of the Au(111) surface, it had been reported that the top layer of gold atoms forms a uniaxial incommensurate rectangular phase at the relatively negative potential by capacity-potential curve,[86] STM,[87] and *ex situ* LEED[88] measurements. This phase is denoted ($p \times \sqrt{3}$), where p and $\sqrt{3}$ are the repeat distances in units of the nearest-neighbor (NN) distance, as schematically shown in Fig. 1(A).[45] In an SXRD measurement, the ($p \times \sqrt{3}$) reconstruction gives rise to additional in-plane reflections beyond the underlying (1 × 1) reflections (Figs. 1(B) and 1(C)).[45] These are arranged in a hexagonal pattern around the integer reflections.[45,46,71] Figure 2[45,46,71] shows the SXRD profiles measured along the q_r (see Figs. 1(B) and 1(C)) at a series of negatively moving potentials between +0.10 and –0.80 V (vs. Ag/AgCl) in 0.01 M NaCl solution. At the potentials more positive than +0.10 V, only a scattering peak was observed at $q_r = 0$, indicating that the surface is not reconstructed. As the potential was made more negative than +0.05 V, a second peak emerged, which is due to the reconstructed phase. The reconstruction peak position, ($\delta/\sqrt{3}$, $1 + \delta/\sqrt{3}$) (see Figs. 1(B) and 1(C)), changed outward corresponding to increased compression as the potential was made more negative.

In addition to the potential region of the reconstruction formation/lifting transition, we investigated the Au(111) surface over a wider potential range (between 0 and +1.40 V) in the normally observed cyclic voltammogram (CV) in 50 mM H_2SO_4 solution (Fig. 3) by using the CTR method.[85] The potential range of the results of Ocko *et al.* as described above corresponds to that between 0 and +0.60 V in this CV (Fig. 3).

At 0 V just after dipping the electrode, our CTR result showed that the interfacial structure is the Au(111)−($23 \times \sqrt{3}$) reconstructed structure covered with 0.74 ML of oxygen species, confirming the results of Ocko *et al.*[45,46,71] At +0.95 V, which is more positive than the potential of the current spikes around +0.90 V, which corresponds to the order/disorder transition of the adsorbed sulfate anion, the CTR result shows that the Au(111)−(1 × 1) surface was covered with the first, second, and third layers composed of 0.88 ML of oxygen, 0.22 ML of sulfur, and 0.24 ML of oxygen species, respectively. The distances between the outermost Au layer and first, the first and second, and the second and third

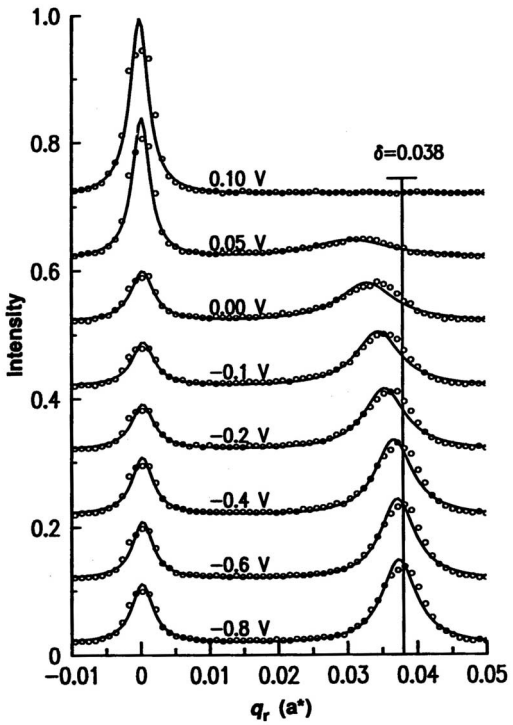

Fig. 2 Representative X-ray scattering profiles along the q_r axis at L = 0.2 in 0.01 M NaCl solution at various potentials chosen from scans between +0.01 and –0.08 V (vs. Ag/AgCl). The solid lines are fits to Lorentzian line shape. The effective scan rate is 0.5 mV s^{-1}. Reprinted with permission from Ref. 45, Copyright American Physical Society (1992).

layers were 2.37, 1.08, and 1.86 Å, respectively. These numbers are in good agreement with those estimated from a model proposed by Kolb *et al.* based on STM[89] and by Ataka and Osawa based on IR.[32] They suggested that the sulfate anion (SO_4^{2-} and/or HSO_4^-) and hydronium ion (H_3O^+) were coadsorbed on the Au(111)−(1 × 1) surface with a ($\sqrt{3} \times \sqrt{7}$)*R19.1*° structure with a molar ratio of 1 : 1 through three oxygen atoms and three hydrogen atoms, respectively. Yoshimoto *et al.* recently investigated by *in situ* STM the structures of the adsorbed sulfate anion in detail.[90] The SXS results also suggested the relatively rough surface of the Au(111)−(1 × 1) as a result of a lifting of the ($23 \times \sqrt{3}$) reconstructed structure.

At +1.05 V, where very small anodic current flowed (Fig. 3), the CTR result showed that the Au(111)−(1 × 1) substrate was covered with the first, second, and third layers composed of 1.00 ML of gold, 0.040 ML of gold, and 1.00 ML of oxygen species. This result indicated that the adsorbed sulfate anion at +0.95 V was desorbed and oxygen species were adsorbed onto the Au(111)−(1 × 1) surface. The height of the oxygen species layer calculated from the present data was ca. 2.3 Å. This value was closely matched with the calculated value (2.14 Å) when the oxygen atom was adsorbed at the on-top site of the Au substrate. Although there have been many discussions on the nature of the adsorbed oxygen species (i.e., O, OH, OH^-, H_2O, H_3O^+, etc.) in this

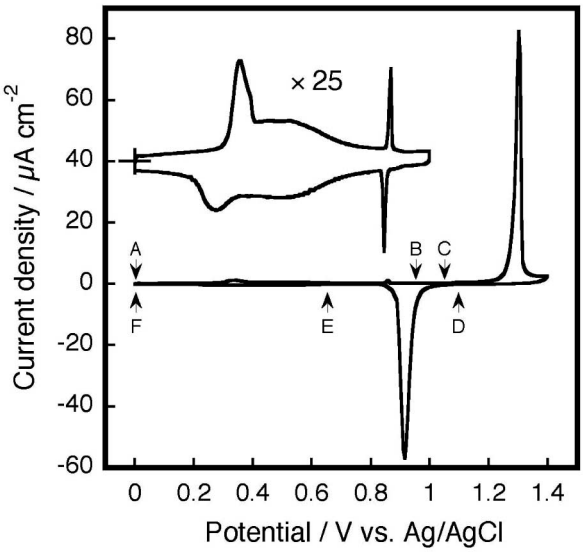

Fig. 3 A CV at the Au(111) electrode measured in a 50 mM H_2SO_4 with a scan rate of 20 mV s^{-1}. Inset: A CV with an expanded current scale in the potential range of 0 through +1.00 V and measured with a scan rate of 5 mV s^{-1}. Arrows A - F represent the potentials where CTR measurements were carried out. Reprinted with permission from Ref. 85, Copyright American Chemical Society (2007).

potential region, one cannot distinguish these species based on the SXS results because X-ray is not scattered by hydrogen atoms, but it can be concluded that oxygen species were adsorbed at the on-top site of the underlying Au(111) − (1 × 1) surface.

Because SXS intensity gradually changed with time at +1.40 V, the CTR measurement was carried out at not at +1.40 V but at +1.10 V. At this potential, the CTR result showed that the Au(111) − (1 × 1) substrate was covered with the first, second, and third layers composed of 0.73 ML of gold, 0.31 ML of gold, and 1.00 ML of oxygen species, respectively. Coverage of gold atoms in the first and second layer less than 1 ML showed that gold atoms coexisted with oxygen atoms. This means gold oxide was formed, although we cannot determine the fraction of oxygen atoms in these oxide layers. As a result of the penetration of oxygen atoms into the gold surface layers, the distances between the outermost layer of the gold substrate and first layers and between the first and second layers were 2.90 and 2.50 Å, respectively, and were larger than the value (2.36 Å) of the bulk Au(111). This result supports the model proposed by Conway *et al.* based on the results of conventional electrochemical measurements that the two-atom thick oxide layer was formed as a result of a turnover reaction.[91,92] The total number of gold atoms in these oxide layers was equivalent to 1.04 ML, which was exactly the same as that of the gold coverage of the reconstructed Au(111) − (23 × $\sqrt{}$ 3) surface observed at 0 V. This indicates that only the gold atoms in the outermost layer are electrochemically oxidized in the potential cycle up to +1.40 V. This result also confirms that the real surface area can be calculated from the charge of the current peak of the oxide reduction.[93]

At +0.65 V, which is more negative than that of the oxide reduction peak (Fig. 3), after the positive-going scan to +1.40 V, the CTR result showed that the first, second, and third layers on the Au(111) − (1 × 1) substrate were composed of 0.87 ML of oxygen, 0.22 ML of sulfur, and 0.24 ML of oxygen species, respectively. These values matched well with those obtained at +0.95 V in the positive-going scan as described above. Furthermore, all the distances between the layers were also in good agreement with those obtained at +0.95 V. Thus, the interfacial structure at this potential is same as that obtained at +0.95 V in the positive-going scan, indicating that the sulfate and H_3O^+ were coadsorbed with a $(\sqrt{3} \times \sqrt{7})R19.1^\circ$ structure through three oxygen atoms and three hydrogen atoms, respectively. One must note, however, that the lateral order of the adsorbates cannot be confirmed based only on this CTR data.

At 0 V after a potential cycle, the CTR result showed that the Au(111) − (23 × $\sqrt{3}$) reconstructed surface was covered with 0.99 ML of oxygen species, as was observed at 0 V before the potential cycle, as described above. The comparison of the structural parameters measured at 0 V before and after the potential cycle showed that the distances between the outermost substrate and first and the first and second layers, coverage of O and Au atoms in the outermost two layers, and RMS values of the all three layers became slightly larger after the potential cycle. These results indicate that small Au clusters existed on the reconstructed Au(111) − (23 × $\sqrt{3}$) surface (i.e., the surface was roughened). This is in good agreement with the well-known fact that once the gold electrode surface is oxidized, oxygen atoms penetrate into the outermost gold layer and the electrode surface is roughened even after the complete reduction of the surface oxide.[84-96]

The same trends of the Au(100) electrodes were also reported.[85]

3 Electro-catalysis on High-Index Planes

Nagahiro HOSHI

High-index planes play a key role in the estimation of the adsorption sites of adsorbates and the active sites for catalytic reactions, because their surface structures can be modified systematically. Figure 4 shows hard sphere models of the representative high-index planes of fcc metals. In the notation such as *n*(111)-(111), the value of *n* shows the number of terrace atomic rows, miller indices after *n* and hyphen indicate the structure of terrace and step, respectively. The high index planes of Pt can be characterized with the use of voltammograms.[97,98] Electricity of the peak due to the adsorbed hydrogen is proportional to the terrace and step atom density on the high index planes of Pt.[99-103] Redox peaks of adsorbed Bi and Ge also depend on the terrace and step structures significantly.[104-107] The low- and high-index planes of Ir[108] and Rh[109,110] also give voltammograms characteristic of their orientation in the adsorbed hydrogen region.

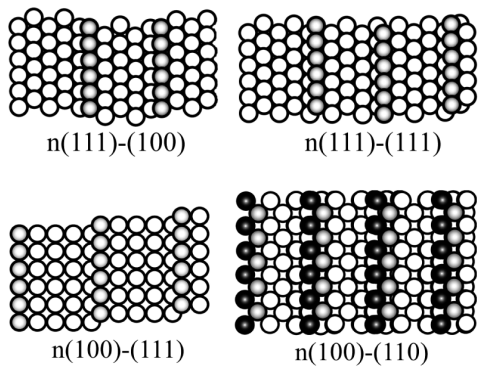

Fig. 4 Hard sphere models of the high index planes of fcc metals.

Volatmmograms of Pd single crystal electrodes depend on the surface structures in both adsorbed hydrogen region[111,112] and oxide film formation region.[111-113]

Voltammograms indicate that the most single crystal surfaces of Pt have unreconstructed (1 × 1) structures. Real surface structures of the low-index planes of Pt were determined in electrochemical environments using STM and SXS. Pt(111) and Pt(100) have unreconstructed (1 × 1) structure,[114-118] whereas Pt(110) has (1 × 1) or (1 × 2) structure depending on the cooling condition after the annealing.[119,120] Surface structures of the high index planes were reported only in UHV,[121] and they reported that *n*(100)-(110) surfaces are facetted. Recently, real surface structures of the high index planes of Pt have been determined with the use of SXS in electrochemical environments. Pt(311) = 2(100)-(111) has reconstructed (1 × 2) structure,[122] but Pt(310) = 3(100)-(110) has unreconstructed (1 × 1) structure.[123] No faceting was found on Pt(310), which is contrary to the case in UHV. Reconstruction to (1 × 2) will not be lifted on the surfaces with $n \geq 3$.[123]

In this section, catalytic reactions, which are related with fuel cell reactions, are briefly summarized on the low- and high-index planes of Pt and Pd. Although many important topics are found in the literature on the thin film on well-defined surfaces, single crystal alloy electrodes and poly-crystalline electrodes, these topics are not included in this chapter because of the page limitation.

3. 1 Hydrogen oxidation reaction

Hydrogen oxidation reaction (HOR) is the anodic reaction of the hydrogen-oxygen fuel cell. HOR proceeds according to the following mechanism:

$$H_2 \rightarrow \begin{cases} H_{ad} + H_{ad} & \text{(Tafel step)} \\ H_{ad} + H^+ + e^- & \text{(Heyrovski step)} \end{cases} \rightarrow H^+ + e^- \quad \text{(Volmer step)}$$

In the early stage of the electrochemistry using single crystal electrodes, HOR and hydrogen evolution reaction (HER) on Pt were reported to be insensitive to surface structure. Afterwards, Marković *et al.* found that the rate of HOR depends on the crystal orientation: Pt(111)< Pt(100)< Pt(110),[124,125] showing step is the active site for HOR. Intermediate species of HOR and HER is the overpotentially deposited (OPD) hydrogen on the on-top site of Pt.[126-128] The OPD hydrogen differs from the underpotential deposited (UPD) hydrogen that gives characteristic peaks in the voltammogram in the adsorbed hydrogen region, because no on-top hydrogen is observed in the adsorbed hydrogen region. However, UPD hydrogen is a spectator species which can block the adsorption of H_2. Thus, the structure sensitivity of the HOR is attributed to the structure sensitive adsorption of H_{ad}.[129] Surface structure also affects the reaction mechanism and the rate determining step (rds) of HOR:

Pt(111): Tafel step → Volmer step (rds)[130]
Pt(100): Heyrovski step (rds) → Volmer step[124,125]
Pt(110): Tafel step (rds) → Volmer step[124,125]

Study on HOR is now extended to the stepped surfaces of Pt for the elucidation of the detailed reaction mechanism.[131]

HOR has not been studied on single crystal electrodes of Pd. Pd absorbs large amount of hydrogen into the bulk. The surface structure of Pd will be distorted by the hydrogen absorption; it is impossible to analyze the correlation between the surface structure and HOR.

Recently, the first-principles molecular dynamics simulation of HER has been done on Pt(111) at which a bias voltage is taken into account in water.[132] They revealed the microscopic details of the Volmer step of HER. Such a calculation will give a deeper insight of HER and HOR.

3. 2 Oxygen reduction reaction

Oxygen reduction reaction is the cathodic reaction of the fuel cell. Structural effects on the oxygen reduction reaction (ORR) were firstly reported by Marković and Yeager *et al.* on the low index planes of Pt.[133] Following activity series of ORR was obtained in $HClO_4$ in which no anion is strongly adsorbed on the electrode surfaces: Pt(100)< Pt(111)< Pt(110).[125,133] Other papers also reported the highest activity of Pt(110).[134-139] According to the study using rotating ring disc electrode (RRDE), four electron pathway ($O_2 + 4H^+ + 4e^- \rightarrow 2H_2O$) is found for ORR above adsorbed hydrogen region on all the low index planes, whereas two electron pathway ($O_2 + 2H^+ + 2e^- \rightarrow H_2O_2$) is observed on Pt(111) and Pt(100) in the adsorbed hydrogen region.[125,133]

The activity of ORR decreases in H_2SO_4, especially on Pt(111). The activity series is reversed between Pt(100) and Pt(111) in H_2SO_4: Pt(111)< Pt(100)< Pt(110).[125] This is because (bi)sulfate anion is adsorbed strongly on Pt surfaces above 0.15 V (RHE).[140] Infrared reflection absorption spectroscopy (IRAS) can predict the adsorption geometry of (bi)sulfate anion on the basis of the selection rule.[141] (Bi)sulfate anion is adsorbed on Pt(111) with three-fold geometry which agrees with the geometry of atomic arrangement of Pt(111) (Fig. 5).[141-147] On Pt(110) and Pt(100), two-fold geometry is proposed (Fig. 5).[148,149] The remarkable deactivation on Pt(111) may be attributed to the three-fold geometry of (bi)sulfate anion that blocks more Pt atoms than two-fold geometry.

ORR was studied on the high-index planes of Pt (*n*(100)-(111), *n*(111)-(100),[150] *n*(111)-(111) and *n*(110)-

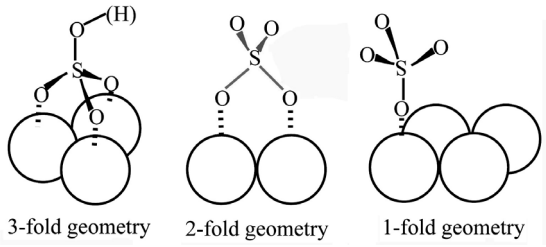

Fig. 5 Adsorption geometry of (bi)sulfate anion.

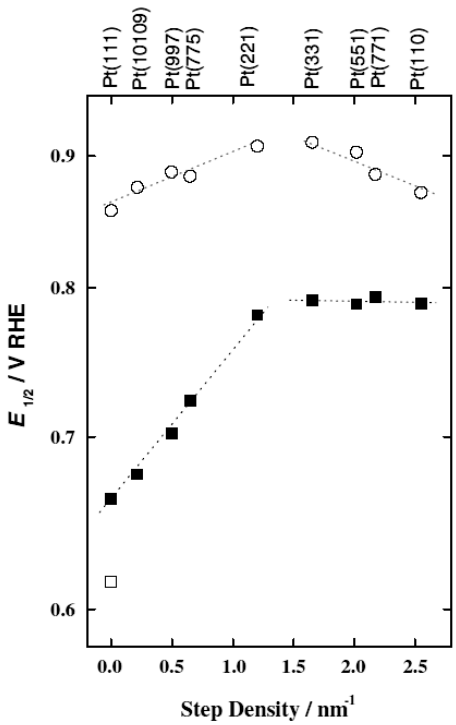

Fig. 6 Structural effects on the oxygen reduction reaction on *n*(111)-(111) and *n*(110)-(111) surfaces of Pt. Reprinted with permission from Ref. 151, Copyright Elsevier Science (2007).

(111)[151]) in 0.5 M H_2SO_4 and 0.1 M $HClO_4$. On *n*(111)-(100) surfaces, exchange current density of ORR increases with the increase of step atom density, giving maximum value on Pt(211) $n = 4$.[150] The same tendency is found on *n*(111)-(111) surfaces, of which activity is estimated using the potential at a current density of a half diffusion limiting value ($E_{1/2}$) (Fig. 6).[151] On *n*(100)-(111) and *n*(110)-(111) surfaces, however, the structural effects on ORR are less significant. The structural effects in H_2SO_4 are more sensitive than in $HClO_4$. This is attributed to the (bi)sulfate adsorption. IRAS study shows that (bi)sulfate anion is adsorbed on the step with two-fold geometry on stepped surfaces of Pt.[140] Activity series of the low-index planes and stepped surfaces indicates that step is the active site for oxygen reduction. It is probable that the coverage or adsorption strength of (bi)sulfate anion at the step depends on the terrace width remarkably. No structural effect is observed on *n*(110)-(111) surfaces in H_2SO_4. No terrace structure exists on these surfaces, because (110) structure is composed of monatomic (111) steps. Lack of the structural effect may be attributed to the lack of terrace structure.

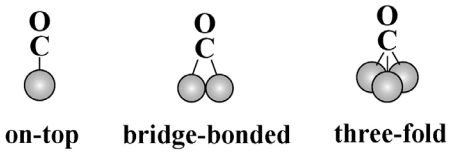

Fig. 7 Adsorption sites of CO.

The difference of the activity for the stepped surfaces is smaller than for the low-index planes in $HClO_4$. This lower structural effect is ascribed to OH adsorption at the step. The higher adsorption energy for oxygen on the step is counterbalanced with higher adsorption strength of the OH species.[150]

ORR study is now extended to the low- and high-index planes of Pd.[152]

3. 3 Nature and oxidation of adsorbed carbon monoxide

Adsorbed CO is poisonous species for catalytic reactions. It is important to find out the active structure for adsorbed CO oxidation for the development of electrocatalysts with high CO tolerance. A huge number of studies was reported on the CO oxidation on platinum electrodes; the topics are focused on the IRAS study of CO adsorbed on the well-defined surfaces of Pt in electrochemical environments. IRAS spectra of adsorbed CO were firstly reported on the low-index planes of Pt in 1987 and 1988.[153-155] Adsorption sites of CO (Fig. 7) depend on the surface structure at saturation coverage. On-top and three-fold CO are found on Pt(111) at lower potentials. Site conversion from three-fold to bridge-bonded CO occurs at higher potentials.[153,154] On-top and asymmetric bridge-bonded CO are observed on Pt(100),[156-158] only on-top CO is adsorbed on Pt(110).[159] IR band of on-top CO dominates the spectra on all the low index planes at saturation coverage. However, STM study shows that the number of on-top CO is the half of multi-bonded CO in the (2×2) adlayer on Pt(111).[160] Intensity transfer occurs from multi-bonded CO to on-top CO due to the dynamic dipole-dipole coupling.[160]

IRAS of adsorbed CO has been also studied on stepped surfaces of Pt in electrochemical environments.[161-167] Adsorbed CO occupies the step site at lower coverage.[161,165-168] Adsorbed CO on step gives an IR band at lower frequency than that on terrace. The band of adsorbed CO on the step cannot be distinguished from that on the terrace at high coverage due to the strong dipole-dipole coupling.[161,165-168] Structural effects on the adsorption site of CO are found on *n*(111)-(111) surfaces of Pt at saturation coverage.[163,164] The IR bands of on-top and three-fold CO appear on the surfaces with the number of terrace atomic rows $n \geq 9$, whereas no three-fold CO is observed on the surfaces with $n \leq 8$.[164] The same tendency was also reported by Koper *et al.*, but three-fold CO was found on the surfaces with $n \leq 6$ in their report.[163] Site conversion from three-fold to bridge-bonded CO is not observed on *n*(111)-(111) surfaces at higher potentials.

According to the anode stripping voltammetry, the peak potential of adsorbed CO oxidation shifts negatively

with the increase of the step atom density on *n*(111)-(111) surfaces of Pt.[169,170] Coverage of adsorbed CO (θ_{CO}) affects the peak potential of the oxidation: lower coverage gives the oxidation peak at more negative potential. However, θ_{CO} increases with the increase of the step atom density on *n*(111)-(111) surfaces.[164,170] These results clearly show that step is the active site of adsorbed CO oxidation. A high-resolution STM image shows that adlayer structure of adsorbed CO on the terrace edge of Pt(100) is different from that on the terrace, indicating different electronic structure of the step and edge.[116]

The oxidation of adsorbed CO on kink is studied on *n*(100)-(110) surfaces of Pt.[168] Kink is defined as protruded atoms in the step line as shown in the black spheres in Fig. 4. CO is adsorbed on only kink on *n*(100)-(110) surfaces of Pt at $\theta_{CO} \leq 0.2$. IR spectra shows that Pt(910) $n = 9$ and Pt(510) $n = 5$ have co-adsorb water at the terrace. Pt(210) $n = 2$, which has no terrace, has no co-adsorbed water. IR band of on-top CO diminishes due to the oxidation above 0.3 V (RHE) on Pt(910) $n = 9$ and Pt(510) $n = 5$ in harmony with the decrease of water band. On Pt(210) $n = 2$, however, on-top CO remains even at 0.60 V (RHE). Adsorbed CO is not oxidized at 0.30 V (RHE) on *n*(100)-(111) surfaces that has no kink atoms at the step.[161] These results support that kink atoms accompanied with co-adsorbed water have high activity for adsorbed CO oxidation.

Some papers claim that adsorbed CO is oxidized by adsorbed OH according to Langmuir-Hinshelwood reaction.[171-173] On the other hand, some papers report that adsorbed CO abstracts oxygen from adsorbed water.[174-177] SEIRAS clearly shows that water band is diminished with the decrease of CO band intensity.[177] No adsorbed OH band was found even with SEIRAS method that has extremely high sensitivity. However, there has been no consensus on the oxidation mechanism of adsorbed CO.

IRAS spectra of adsorbed CO were also reported on the low- and high-index planes of Pd.[178-182] Bridge-bonded CO dominates the spectra. On-top CO is mainly adsorbed on the step. On-top CO on the terrace is found on only large (111) terrace with $n \geq 20$.[182] No site conversion of CO is observed. CO oxidation on the high-index planes of Rh was studied using voltammetry and chronoamperometry.[110,183,184]

3. 4 Oxidation of formic acid and methanol

Formic acid is an intermediate of methanol oxidation, and it also works as fuel of direct formic acid fuel cell. Oxidation of formic acid was believed to proceed via the dual path mechanism: poisonous and reactive intermediates are formed during the reaction. IRAS studies have shown the poisonous intermediate is adsorbed CO,[185-187] and SEIRAS verifies the reactive intermediate is adsorbed formate (HCOO).[188-190]

Many papers reported formic acid oxidation on single crystal electrodes of Pt.[191-194] When the activity is estimated from the anodic peak current density in the first positive scan after the annealing, following activity series is obtained for the oxidation ($HCOOH \rightarrow CO_2$): Pt(100)< Pt(111)< Pt(110).[194] High activity of Pt(110) indicates that step is the active site for formic acid oxidation. Sun *et al.* studied the oxidation on *n*(100)-(110) surfaces of Pt.[195] They estimated the initial rate of dissociative adsorption of formic acid ($HCOOH \rightarrow CO_{ad}$) with the use of current-time transient curves, giving the following activity series: Pt(610) $n = 6$ < Pt(100)< Pt(210) $n = 2$ < Pt(110). This result also shows step (kink) enhances the dissociative adsorption of formic acid.

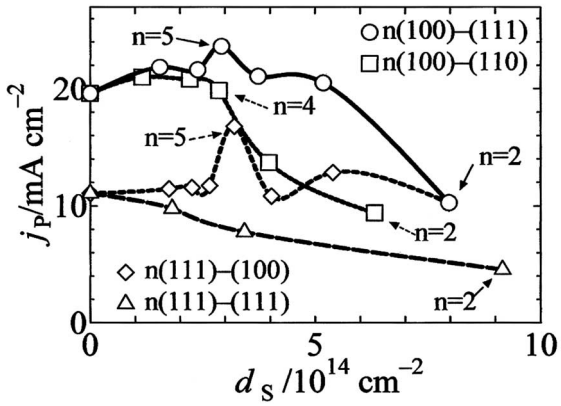

Fig. 8 Step density dependence on the oxidation rate of formic acid on the high index planes of Pd. Reprinted with permission from Ref. 203, Copyright Elsevier Science (2007).

Pd electrodes have advantage for formic acid oxidation compared with Pt electrodes: no poisonous intermediate (adsorbed CO) is formed on Pd electrodes during formic acid oxidation.[196] Therefore, the onset potentials of formic acid oxidation on Pd electrodes are much more negative than those on Pt electrodes. SEIRAS detected adsorbed formate during formic acid oxidation on a thin film of Pd on Au electrode,[197] but another paper using SEIRAS found no adsorbed formate.[198] There is no solid evidence for the intermediate species of formic acid oxidation on Pd electrode at present. The activity series on the low index planes of Pd is as follows: Pd(111)< Pd(110)< Pd(100) in 0.5 M H_2SO_4,[199] Pd(110)< Pd(111)< Pd(100) in 0.1 M $HClO_4$.[200] Flat Pd(100) surface has highest activity for formic acid oxidation. The oxidation rate on Pd(111) gets lower in H_2SO_4 compared with that on Pd(110). (Bi)sulfate anion is adsorbed with three-fold and one-fold geometry on Pd(111) and Pd(110), respectively, and coverage of the anion on Pd(111) is higher than that on Pd(110).[201,202] The difference of the adsorption geometry and coverage causes the significant deactivation of Pd(111) in H_2SO_4.

Formic acid oxidation was studied on the high index planes of Pd in 0.1 M $HClO_4$.[200,203] Anodic peak current density of formic acid oxidation ($HCOOH \rightarrow CO_2$) is plotted against the density of step atoms in Fig. 8. Pd(911)= 5(100)-(111) has the highest rate for the oxidation. The values of j_P (anodic peak current density) on *n*(100)-(111) and *n*(100)-(110) are as high as that on Pd(911)= 5(100)-(111) on the surfaces with terrace atomic rows $n \geq 3$ or 4. These results indicate that (100) terrace with atomic rows more than 3 or 4 is appropriate reaction field for formic acid oxidation.

Methanol oxidation on Pt electrodes also proceeds via the dual path mechanism. Poisonous and reactive inter-

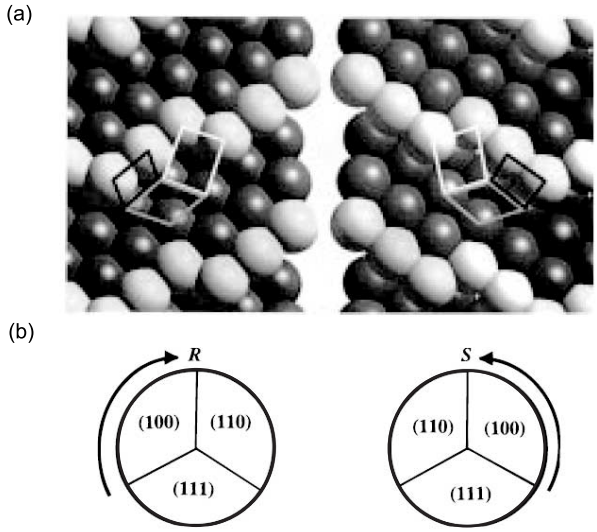

Fig. 9 (a) Hard sphere models of chiral surfaces: Pt(643)^S and Pt(643)^R. The (111) (gray line), (110) (white line), and (100) (black line) sites comprising the kink are indicated. White spheres show the kink edges. (b) Cahn-Ingold-Prelog analogy used to define the absolute stereochemistry of the kink site as either S or R. Reprinted with permission from Ref. 218, Copyright American Chemical Society (1999).

mediate species are adsorbed CO and adsorbed formate, respectively, according to SEIRAS study.[204] Adsorbed formate is also found on Pt(111) and Pt(100) using a flow cell in the conventional IRAS configuration.[205] Activity series of methanol oxidation, which is estimated by the anodic peak current density in the first positive scan, is as follows in acidic solutions (H_2SO_4 and $HClO_4$): Pt(111)< Pt(100)< Pt(110).[206,207] The current density increases in alkaline solution, giving the following order in 0.1 M NaOH: Pt(100)< Pt(111)< Pt(110).[208,209] Pt(110), which has step site, has high activity for methanol oxidation. Methanol oxidation on the high-index planes of Pt indicates that overall oxidation rate of methanol and decomposition of methanol to CO are enhanced by step.[210,211]

3. 5 Oxidation of glucose

Glucose-oxygen fuel cell can be applied to the battery of cardiac pacemakers and artificial heart. Elucidation of surface structures enhancing glucose oxidation is important for this purpose. Mechanism of glucose oxidation was studied on Pt electrodes using IRAS.[212-214] Gluconolactone, carboxylic acid and CO_2 were produced. Activity series of glucose oxidation, which is estimated by the anodic peak current density in the positive scan of the voltammogram, is as follows in acidic solution: Pt(110)< Pt(100)< Pt(111).[215] Pt(111) also has the highest activity in alkaline solution: Pt(100)~ Pt(100)< Pt(111).[216] The oxidation of glucose was studied on n(100)-(111) ($2 \leq n \leq 14, \infty$) surfaces of Pt in 0.1 M $HClO_4$. Anodic current density due to glucose oxidation increases with the increase of (100) terrace width.[217]

One of the interesting topics is the oxidation of glucose on chiral surfaces. Figure 9 shows hard sphere models of chiral Pt(643) surface.[218] Small domains of (111), (100) and (110) form chiral structure as shown in Fig. 9b. Pt(643)^R and Pt(531)^R have higher oxidation rate for L-glucose than D-glucose, showing enantiomeric electrochemical response.[218,219] Other optically active compounds such as mannose, arabinose and xylose also have strong enatiomeric response on chiral surfaces.[220,221] Chiral alkanols, however, show weak enathiomeric response compared with sugars. One of the possible explanations is that molecules having cyclic structures are more likely to meet the necessary geometrical conditions for the observation of enantiomeric effects. It is also probable that the aldehydic carbonyl function on glucose and related molecules hold the key to differences in enantioselectivity.[222]

High-index planes are good models of shape-controlled nanoparticles that can be used for practical electro-catalysts. If active surface structures can be built on nanoparticles, the activity of practical electrocatalysts will be enhanced dramatically. Preparation and electrochemistry of shape-controlled nanoparticles have been studied extensively since Elsayed reported the preparation of cubic and tetrahedral Pt nanoparticles.[223-228] Deeper understanding of the structure and the reaction of high-index planes is important for the elucidation of the origin of the catalytic activity of nanoparticles.

4 EC-STM for Reaction Analysis

Junji INUKAI

EC-STM has been one of the most powerful tools to understand the static structures on electrodes in solution.[3] Recently, it is widely used to investigate various electrochemical reactions,[20] showing even the dynamic features on electrodes.[18,229] Advances in the EC-STM studies on the electrochemical reactions are described in this section.

In vacuum, the topmost surface of Pt(100) is known to be hexagonally reconstructed, in order for the surface energy to be lowered (Fig. 10).[230] This reconstructed surface is called Pt(100)-hex-R0.7°. The reconstruction of Pt(100), as well as Au(100), was historically started to be investigated by the use of LEED after the sample was emersed from solution into vacuum. After Clavilier and coworkers reported the powerful, yet convenient method to expose well-defined Pt surfaces in solution,[5] Pt(100) surface became widely used for precise electrochemical studies.[231] *In-situ* X-ray reflectivity measurements were then carried out on a clean Pt(100) surface immersed in solution,[117] and EC-STM was next applied to the Pt(100) electrode.

In situ STM revealed that the Pt(100) surfaces prepared by flame annealing followed by slow cooling in a H_2 stream exhibit atomically flat terrace-step features in a 0.1 M $HClO_4$ solution.[232] Atomically flat terraces extended over several hundreds of nanometers in width, and straight monatomic-height steps are positioned mostly in the < 110 > direction (Fig. 11a). On an atomically flat terrace, atomic images of the Pt(100)-(1 × 1) structure were obtained at a potential near the hydrogen evolution reaction almost perfectly: the unreconstructed Pt(100) surface was exposed by the flame annealing and

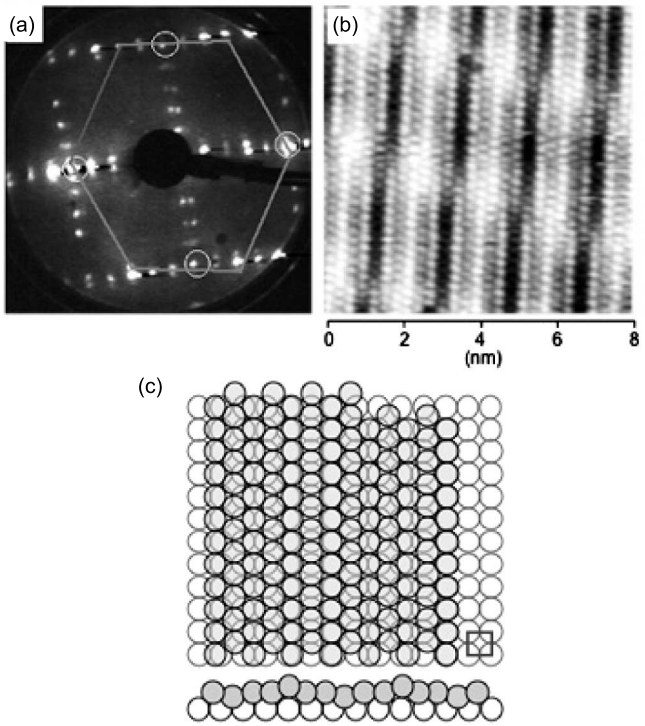

Fig. 10 LEED pattern (a) and STM image (b), and structural model (c) for Pt(100) reconstructed surface obtained in vacuum. Hexagon shows (1 × 1) spots. Reprinted with permission from Ref. 233, Copyright The Electrochemical Society (2003).

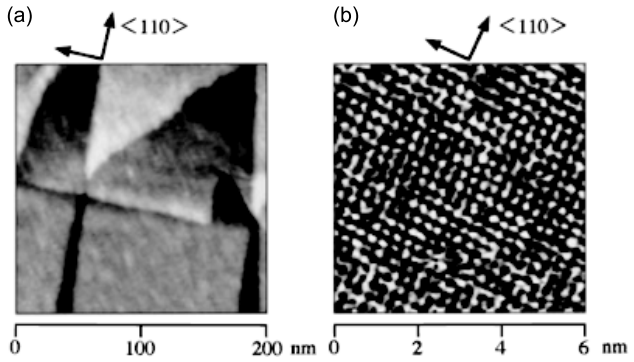

Fig. 11 Large-scale (200 nm × 200 nm) (a) and high-resolution (6 nm × 6 nm) (b) *in-situ* STM images of Pt(100) in 0.1 M $HClO_4$. The sample potential was 0.15 V vs. RHE, and the tunneling current, 26 nA. Reprinted with permission from Ref. 232, Copyright American Chemical Society (1998).

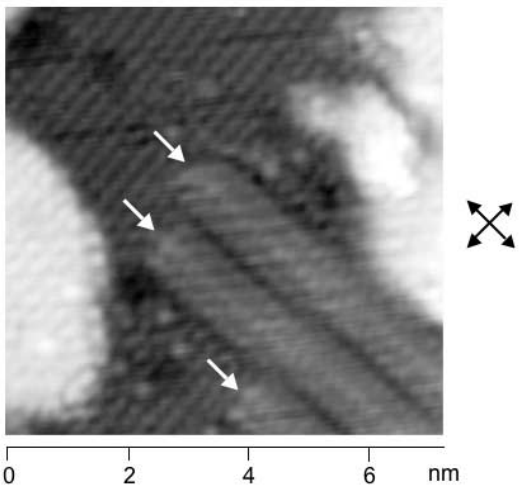

Fig. 12 STM image of Pt(100) emersed from a 5 mM H_2SO_4 at 0.2 V vs. RHE. Reprinted with permission from Ref. 233, Copyright The Electrochemical Society (2003).

quenching method (Fig. 11b).

In order to understand the different surface structures on Pt(100) in vacuum and in solution, the Pt(100)-hex-R0.7° was prepared in vacuum, transferred into solution, and electrode potentials were applied. Then, the Pt sample was transferred back into vacuum to be examined by LEED and STM.[233] Figure 12 shows the STM image of the Pt(100) surface emersed from solution at the electrode potential of 0.2 V vs. RHE. It is clearly seen that the most of the surface was changed to (1 × 1) after the adsorption of hydrogen atoms in solution. Also seen are the reconstruction domains remained, which are shown by arrows in Fig. 12. In this way, STM solved a long lasting issue of the reconstruction of Pt(100) surface: hydrogen adsorption lifts the Pt(100) surface to (1 × 1) from hex-R0.7°. It was also revealed that the adsorption of hydrogen atoms from a gas-phase hydrogen, H_2, changes the surface from hex-R0.7° to (1 × 1).[233] In the case of the EC-STM observation in solution (Fig. 11), the sample was slowly cooled down under hydrogen after the annealing. In this way, the surface is expected to have been slowly flattened to have wide terraces (Fig. 11a) with hydrogen atoms adsorbed on the surface. At a low electrode potential in solution, the hydrogen atoms remained attached on the surface, and the (1 × 1) structure was observed by EC-STM (Fig. 11b). The hydrogen adsorption was thus correlated with the phase transition of the Pt(100) surface by EC-STM.

Now, dynamic approaches are needed to understand the kinetics of the phase transition. Magnussen and coworkers have developed a high-speed electrochemical STM, which allows one to obtain atomic resolution images at acquisition rates up to 25 images per second.[234] By using this high-speed STM (video-STM), the dynamic behavior was observed of five-atom-wide, hexagonally ordered strings of Au atoms embedded in the square lattice of the Au(100)-(1 × 1) surface.[229] A quasi-collective lateral motion of these strings was found both along the strings and in the direction perpendicular to them. The perpendicular motion can be ascribed to small atomic displacements in the strings induced by propagating kinks. These defects were also suggested to provide a mechanism for the exchange of Au atoms between the two string ends, required for motion in string direction.

Atomic-scale dynamic processes during Cu(100) dissolution/deposition in 0.01 M HCl solutions were also studied by video-STM.[235] Figure 13 shows a sequence of consecutive images from a video recorded in a solution containing 2×10^{-6} M Cu ions. The equilibrium fluctuations

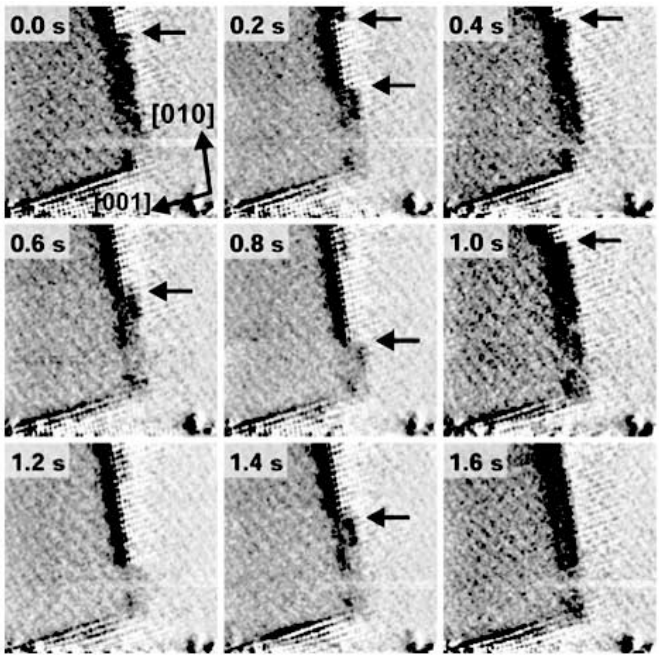

Fig. 13 Series of *in situ* video-STM images (19.0 nm × 11.5 nm) recorded on Cu(100) in 0.01 M HCl + 2×10^{-6} M $CuSO_4$ at –9 mV vs. Cu/Cu(I). Reprinted with permission from Ref. 235, Copyright The Royal Society of Chemistry (2002).

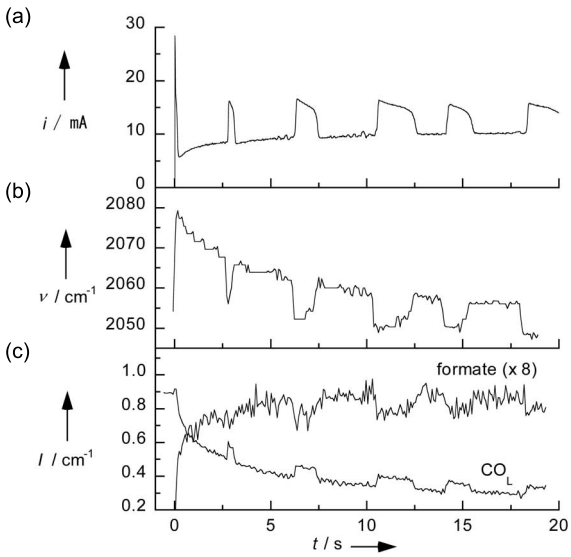

Fig. 14 (a) Current oscillations observed in formic acid oxidation at a constant potential of 1.1 V (RHE) in 0.5 M H_2SO_4 + 1 M HCOOH with an external resistor of 30 Ω. (b) Vibrational frequency of linear CO (CO_L) and (c) integrated band intensities of CO_L and formate taken from a series of SEIRA spectra acquired simultaneously with the current-time curve. Reprinted with permission from Ref. 241. Copyright Wiley-VCH Verlag GmbH & Co. KGaA (2005).

at atomic kinks in the steps on the crystal surface are directly observed due to the local removal/addition of atoms. The same anisotropic behavior was also found in Cu-free electrolytes, caused by the influence of the ordered (2 × 2)-Cl adlayer on the kink structure. In this way, EC-STM, known as its high spatial-resolution, is now given a high time-resolution.

To understand the relationship between structures and reactivities, modifications of single-crystal surfaces are carried out with the help of EC-STM. Wieckowski and coworkers have been imitating catalyst surfaces of fuel cells by depositing additional metals on single-crystal surfaces, such as, Ru and Os on Au(111) and Pt(111).[236,237] Coverage and morphology of metal islands on Au and Pt surfaces were directly observed by EC-STM, and reaction mechanisms have been discussed on those model electrodes.

Electrochemical oxidation of CO is another important topic, especially in the field of fuel cells. The reaction mechanism of CO oxidation has been investigated by the use of EC-STM. Wakisaka *et al.* reported the structures of CO adlayers on Pt(100) and discussed the reaction mechanism on the surface.[116] Rhee and coworkers have proposed new adlayer structures of CO on Pt(111) and discussed the reaction mechanism at the pre-oxidation peak.[238]

EC-STM is now considered to be a tool not only for determining electrode structures but also for analyzing electrochemical reactions.

5 Real-Time Monitoring of Electrochemical Surface Reactions and Dynamics by Time-Resolved SEIRAS

Masatoshi OSAWA

Many in situ surface analytical techniques are now available as has been described in the previous sections, but few of them have time resolutions high enough to monitor fast surface reactions. Infrared spectroscopy is suited for this purpose. Ito and co-workers[156] realized ms time-resolved IRAS monitoring for the first time and demonstrated that CO adsorbed on Pt(100) surface reversibly change its adsorption site within ~100 ms for a potential step. Nevertheless, the response of the system with respect to the externally applied perturbation is slow in the IRAS setup using a thin solution layer. Additionally, limited mass transport between the thin layer and the reservoir makes the detection of reaction intermediates difficult because reactants are quickly consumed and products are accumulated in the thin layer.[239] SEIRAS in the ATR mode using a prism/metal/solution configuration is free from such problems.[31,240] Higher sensitivity is an additional advantage of SEIRAS and facilitates time-resolved monitoring of electrochemical reactions and dynamics simultaneously with electrochemical measurements.

Electrochemical oscillations are good examples for demonstrating the necessity of time-resolved monitoring. As is found in Fig. 14a, oxidation current spontaneously oscillates during potentiostatic oxidation of formic acid at

Pt electrode. SEIRAS observation of the electrode surface with 80-ms time resolution revealed that CO and formate are adsorbing on the surface and change their band intensities (i.e., coverages) synchronously with the current oscillations (Fig. 14c).[241] Additionally, the temporal change of the vibrational frequency of linear CO (Fig. 14b) indicates that the potential at the surface, ϕ (= E-iR) is also synchronously oscillating (red- and blue-shift correspond to the decrease and increase, respectively, in ϕ) apparently due to the change in ohmic drop. The result was interpreted in terms of the so-called dual pathways mechanism: Formic acid is oxidized to CO_2 via adsorbed formate (direct pathway) and via adsorbed CO (indirect pathway).[190] Note that the two pathways share the same surface and are kinetically coupled. CO accumulation at low potentials suppresses the direct pathway, while CO oxidation at high potentials activates the direct pathway. By the interplay with the change in ϕ, this cycle repeats itself to give the sustained temporal current oscillations. Potential oscillations during galvanostatic formic acid and formaldehyde oxidation are explained similarly.[189,242]

The time-resolution of FT-IR spectroscopy is determined by the scan rate of the interferometer (typically 20 scans per second in rapid scan mode at the spectral resolution of 8 cm^{-1}). If the system to be examined is reversible, time resolution of FT-IR can be extended to μs by using step scan mode,[243] in which time resolution is limited by that of the A/D converter or the response of the detector. The redox reaction of heptylviologen,[243] and adsorption/desorption of fumaric acid,[244] (bi)sulfate,[245] and *p*-nitrobenzoic acid[246] in the sub-ms range were examined by this technique.

Time-resolution achieved by step-scan FT-IR is high enough for traditional electrochemical approach because the response of the electrochemical systems is limited to 0.1-1 ms for ordinary electrodes due to the double-layer charging. A possible way to circumvent this limitation is the so-called temperature (*T*) jump method using visible or NIR laser pulses.[247] Irradiation with a short pulse suddenly raises the temperatures of the electrode and the interface, which spontaneously change the rest potential (*E*) of the electrode. Current (or potential) transient measurements after a short-pulse irradiation have been used to examine electron transfer kinetics,[248] but such electrochemical monitoring is still limited to the ns-ms time range due to the time constant of the electrochemical equipments.

Very recently, this limitation was removed by monitoring the interface with a ps-pulsed IR laser after visible pump-pulse irradiation.[249,250] Thanks to the high sensitivity of SEIRAS, ps time-resolved IR spectra of CO adsorbed on a Pt electrode were obtained with S/N good enough for qualitative analysis of the *E*-jump induced by a visible laser pulse. Open circles in Fig. 15 shows that the C-O stretch frequency of adsorbed CO is shifted from 2082 to 2076 cm^{-1} within 200 ps after a 30-ps visible pulse irradiation. The shift can be ascribed to the *T*-jump of the electrode surface[251] (0.05 cm^{-1} K^{-1} [252]) and also *E*-jump (30 cm^{-1} V^{-1} [253]). The two contributions

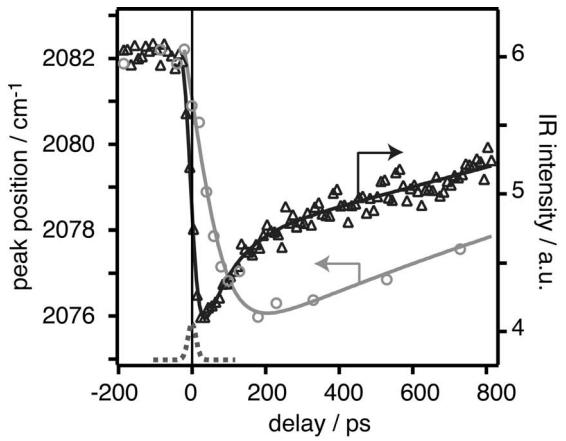

Fig. 15 Temporal profiles of the vibrational frequency of adsorbed CO (circles) and a reflected IR intensity measured at 2000 cm^{-1} (triangles) before and after the irradiation of a 532 nm pump pulse (35 ps, 3 mJ cm^{-2}). The temporal profile of the laser pulse is indicated by the broken line. Reprinted with permission from Ref. 249. Copyright The American Chemical Society (2006).

were successfully separated by the help of the change in the background reflectivity of the electrode (triangles) caused by the heating of the substrate (the increase of the lattice phonon temperature).[251] The shift caused by the *E*-jump was estimated to be –5 cm^{-1} at 200 ps, which corresponds to a potential shift of –150 mV. The *E*-jump occurs by a slight thermal disturbance of water molecules at the interface, and hence it is slightly delayed due to thermal diffusion from the surface to the solution. The same system was also examined by ps time-resolved SFG, in which the shift of the CO vibration was not observed and instead site conversion of CO from atop site to bridge site was observed.[254] Reason of the different results is unknown.

As has been reviewed above, studies using IR spectroscopy are shifting from simple molecular adsorption under potentiostatic conditions to reactions and dynamics.

6 Nonlinear Optical Techniques: SFG/SHG

Shen YE

As described above, structural elucidation and control on the electrode-solution interface is essential to understand the mechanism of the electrochemical reaction. Scanning probe microscope (STM and AFM) and SXS are powerful *in situ* techniques to probe the surface morphology and structure with an atomic resolution. Difficulties are, however, often encountered to explain the physical meaning of the image or adlattice observed by these methods because they do not always provide direct structural information of the adsorbates arranged on the electrode surface. On the other hand, optical methods such as IR spectroscopy, Raman scattering, surface plasmon resonance (SPR) and ellipsometry, can give useful information about the molecular identification, ori-

entation and conformation on the electrode surfaces. Most of these optical techniques are, however, not intrinsically surface-specific, and hence hard to distinguish the contribution from the electrode surface and electrolyte solution. SERS[29] and SEIRAS[31] have been used to detect the surface species but difficulties in sample preparation and quantitative spectral analysis limit their application.

$$\mathbf{P}^{(2)} = \sum_{i}\sum_{j,k} \chi^{(2)}_{ijk} E_j E_k = \chi^{(2)}_{ijk} : EE$$

As 2nd-order nonlinear optical technique, sum frequency generation (SFG)[255] and second harmonic generation (SHG)[255] are attracting much attention in electrochemical science due to their high surface selectivity, sensitivity, and versatile applicability and can provide molecular and electronic structure information on the electrode surface with a sensitivity of sub-monolayer level.[34-42]

The source of SFG is the non-linear polarization $\mathbf{P}^{(2)}$, induced by two laser beams at frequency ω_1 and ω_2, where $\chi^{(2)}$ is the 2nd-order susceptibility as a 3rd-rank tensor consisting of 27 (3^3) elements.[255] The tensor element χ_{ijk} represents Cartesian component i ($i = x, y, z$) of the susceptibility induced by Cartesian components j and k ($j, k = x, y, z$) of the electric field, respectively. Since the field here is the total field applied ($E^{\omega_1} + E^{\omega_2}$), it is easy to know by expanding the above-mentioned equation that $\mathbf{P}^{(2)}$ radiation contains components oscillating at double ($2\omega_1$, $2\omega_2$), sum ($\omega_1 + \omega_2$), difference frequencies ($\omega_1 - \omega_2$) of the two applied fields. The oscillating polarizations will emit lights at diverse frequencies with intensities proportional to the square of each $\mathbf{P}^{(2)}$. This is the origin for the 2nd-order nonlinear optical process such as SFG and SHG where SHG can be regarded as a special case of SFG when $\omega_1 = \omega_2$. Since $\chi^{(2)}$ is invariant in a centrosymmetric material but changes its sign by the inversion operation, $\chi^{(2)}$ must be zero in the bulk medium with inversion symmetry under the electric dipole approximation. Therefore, $\mathbf{P}^{(2)}$ radiation will occur only in non-centrosymmetric materials and at surface or interface where the bulk symmetry is broken, SFG and SHG can be used to probe the interfacial properties of the centrosymmetric materials.

Due to its experimental simplicity, SHG system has been applied in study of the electronic and geometric structures on the electrode surface by fixing ω in visible or near IR region[34,35] since 1980s while SFG system has been developed quickly with the progress in the laser technology in recent years.[41] Usually, SFG is used as vibration spectroscopy where ω_1 is fixed in visible, near-IR or UV region (ω_{vis}) while ω_2 is tunable in IR region (ω_{IR}). As ω_{IR} is equal to local vibration level on the surface, $\chi^{(2)}$ is resonantly enhanced and a peak is observed in the SFG spectrum. By measuring a SFG spectrum as a function of w_{IR}, the vibrational modes of the molecules at the surface / interface can be probed with different polarization combination of SFG, visible and IR. SFG signal can be further enhanced when ω_{vis} and/or ω_{SFG} are also resonant with existing surface states. Details about the theory, experimental system and application for these nonlinear optical techniques have been described elsewhere.[41,258-261]

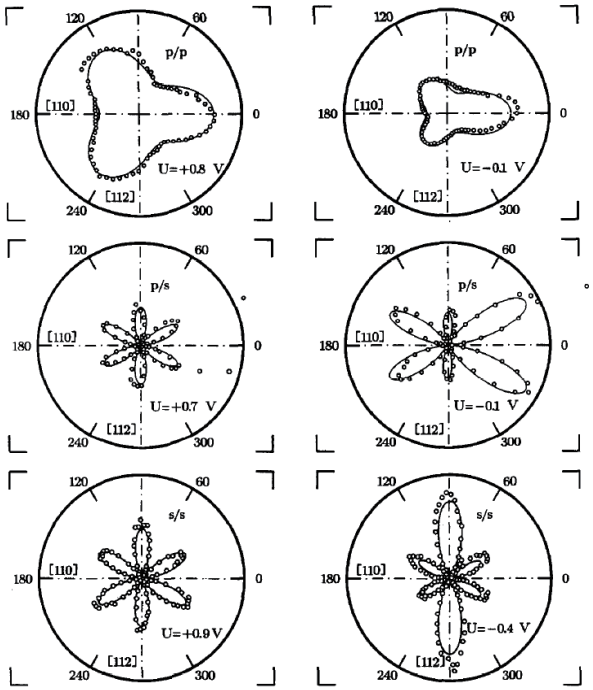

Fig. 16 Polar plots of SHG intensity vs. azimuthal angle (ϕ) of Au(111) electrode in the positive (left) and negative (right) potential regions (pzc = 0.27 V vs. SCE), and for p/p, p/s, and s/s polarization of incident ω- and emitted 2ω-beams. Electrolyte 0.01 M $HClO_4$. Reprinted with permission from Ref. 33, Copyright Elsevier Science (1992).

Since SHG is sensitive to surface symmetry of metal substrate, it has been successfully employed to study UPD of metal, anion adsorption and surface reconstruction on single crystal electrode surface.[34,35] Figure 16 shows polar plots of *in situ* SHG rotational anisotropy measurement on Au(111) electrode in 0.01 M $HClO_4$ solution before (left) and after (right) the surface reconstruction for three different polarization conditions.[33] In the positive potential region (left), the SHG anisotropy patterns exhibit the three-fold rotational axis for all polarizations as expected for Au(111) surface with C_{3v} symmetry, indicating a well-defined (1×1) structure there. In the negative potential region (right), however, the SHG anisotropy is clearly different from that of C_{3v} symmetry. Detailed analysis shows the presence of a new C_v symmetry on the Au(111) surface, corresponding to a ($\sqrt{3} \times 23$) structure. The reversible transition from C_{3v} to C_v rotational symmetry from the SHG-anisotropy patterns with electrode potential is attributed to the lifting and formation of reconstruction on Au(111) surface.[33] The *in situ* SHG measurements also confirmed that anion adsorption can easily lead to the reconstruction on the Au(111) surface (also see Figs. 1～3 in the present review).[33]

On the other hand, SFG spectroscopy is widely used to investigate the structure, symmetry, and ordering of the molecules on the interface which is hard to be obtained by the conventional vibration spectroscopy.[37-42]

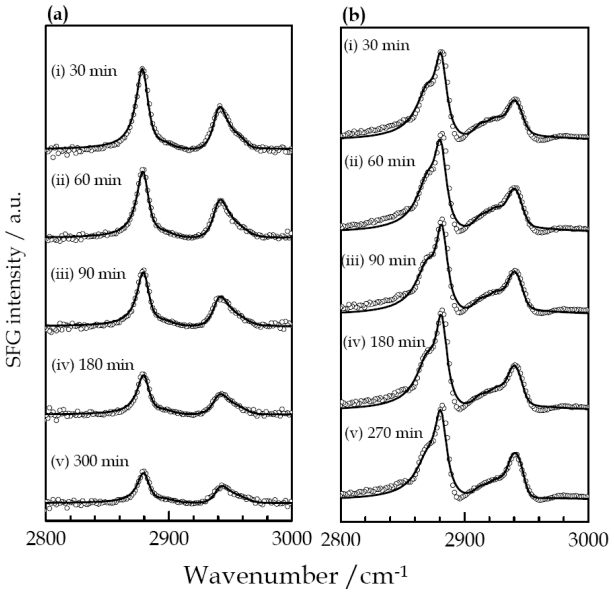

Fig. 17 *In situ* SFG spectra of LB bilayer of deuterated (D) and regular (H) stearic acid on a fused quartz surface in 0.3 mM $NaHCO_3$ with (a) 0.2 mM Cd^{2+} and (b) 0 mM Cd^{2+} for various immersion times. The polarization combination is s-SFG, *s*-Vis, *p*-IR (*ssp*). Reprinted with permission from Ref. 267, Copyright American Chemical Society (2004).

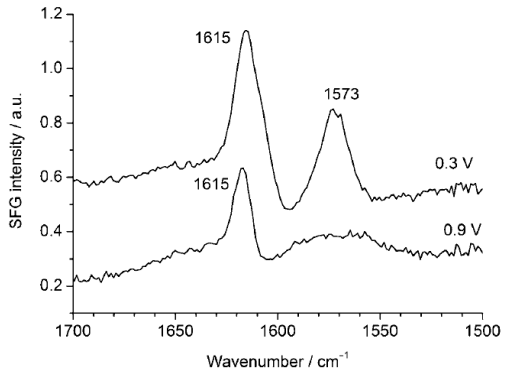

Fig. 18 In situ sum-frequency generation (SFG) spectra of the tri-ruthenium complex SAM on gold electrode surface in 0.1 M $HClO_4$ in the frequency region of the ν_{as}(OCO) vibration at +0.3 V and +0.9 V (vs. SCE), respectively. Each SFG spectrum is co-added over 100 s. Reprinted with permission from Ref. 269, Copyright Wiley-VCH Verlag GmbH & Co. KGaA. (2005).

One of the most successful examples for SFG application is elucidation for structure of water molecules on the interface.[262,263] Although many theoretical studies about the structural properties of water molecules on various interfaces have been carried out, the experimental investigations on the structure of water have been mainly done in vapor or bulk aqueous media due to a lack of effective experimental probes.[264] Shen and co-workers firstly reported the SFG spectra of the water on the air/water and solid/water interfaces.[262,263] A sharp peak was observed at 3680 cm^{-1} at water/air interface or fused quartz surface modified by an octadecyltrichlorosilane (OTS) monolayer, indicating the existence of water molecules without hydrogen bonding. In addition to the free OH group, a broad OH stretching bands of the interfacial water molecules can be also found around 3200 cm^{-1} closely resemble that of a hexagonal ice surface in air, confirming that interfacial water molecules are aligned in a well-ordered structure as a result of the hydrophobic effect. Since the pioneer work, many experimental as well as theoretical researches have been carried out on various water interfaces and largely promote our understanding on the interfacial water structures and properties.[38,42,265,266]

In addition to the surface selectivity, SFG spectroscopy shows several unique features in comparison with IR and Raman spectroscopy. As an example, Fig. 17 shows *in situ* SFG study for reconstruction process of fatty acid bilayer, which is a model system for biomembrane, on solid surface in solution.[256,257,267,268] Since bilayer structure has a centrosymmetry which is SFG-inactive, and hence an asymmetric bilayer system are prepared by successively depositing deuterated (D) layer and regular fatty acid (H) layer (i.e., DH or HD bilayer) to make it SFG-active. Figure 17a exhibits *in situ* time-resolved SFG spectra in the C-H stretching region for a DH bilayer in a 0.3 mM $NaHCO_3$ containing 0.2 mM Cd^{2+}. Two intense peaks around 2875 and 2940 cm^{-1} soon after setup, which can be assigned to symmetric and Fermi-resonance C-H stretching modes of the terminal CH_3 group in the H layer while no peak from CH_2 groups can be observed. Since CH_2 groups become SFG-inactive if the alkyl chains of the fatty acid molecules align in an *all-trans* conformation, this result implies that a well-ordered H layer was constructed here. It is interesting to note that these two SFG peaks became weaker with the immersion process in the solution (Fig. 17a). After 5 hr. immersion, the peak intensities decreased to ca. one third of its original values, suggesting that the structure of the top layer (H) of the DH bilayer significantly changed during the immersion process in the solution. In order to understand the reason for the structural change, SFG experiment was carried out for the DH bilayer in the same solution but without Cd^{2+} (Fig. 17b). In this case, in addition to the strong peaks from CH_3 groups, one may see some weak CH_2 bands around 2850 and 2920 cm^{-1} after bilayer preparation, which may be related to a slightly higher density of gauche defects in the bilayer when Cd^{2+} is not included in solution, the SFG spectrum is generally similar to that in Fig. 17a-(i). It is mostly important issue to note that the intensities of the SFG peaks from CH_3 group are almost constant after long term immersion in the solution (Fig. 17b) which is completely different from those observed in a solution with Cd^{2+}. This feature can be attributed to a structural change on the surface of the fatty acid bilayer induced by the metal cation Cd^{2+}. Due to the strong electrostatic interaction between the carboxylate group with Cd^{2+}, part of the topmost-layer molecules are flipped over to the top of the bilayer gradually forming a new bilayer structure.[267] This process will decrease the symmetry of the original DH bilayer and therefore, SFG signals

decreases with immersion (Fig. 17a). Absence of these changes in the SFG spectra in a solution without Cd^{2+} confirms the influence of the metal cation in solution (Fig. 17b). These structural changes on the surface of fatty acid bilayer can be only sensitively detected by *in situ* SFG measurement in comparison with other convention spectroscopy methods such as IR and Raman.

SFG spectroscopy has been applied as an effective method to study the structure on the electrode and solution interface from early stage of SFG development. The conventional *in situ* IR measurement has a number of disadvantages in electrochemical environment.[41] First, as the species interested exist both in solution and on electrode surface, it is hard to completely distinguish their contribution to IR spectra due to the low surface selectivity of the method; Second, all *in situ* IR spectra on the electrochemical interface are differential spectra which always need a reference spectrum recorded on different potential or under different conditions. It is almost impossible to get absolute structural information from the IR spectra if one does not know the exact structural information in the reference spectra. In fact, such kind of information is not available for most cases on the interface between electrode and solution. Shape and intensity of IR spectra can heavily affected by selection of reference spectrum and explanation will greatly change if the explanation for the reference spectrum is changed. Third, it is hard to investigate the fast reaction dynamics on the electrode surface using FTIR spectrometer due to its time resolution but will be easier for SFG spectroscopy using ultra-short laser pulses.[254] In these aspects, SFG demonstrates its advantage to the IR spectra due its unique feature of nonlinear optical spectroscopy.

SFG measurement directly provides an absolute vibration spectrum since it does not require a reference spectrum (one needs to measure a standard spectrum in SFG measurement to normalize beam overlap and spectral profile but it has different meaning with reference spectrum for *in situ* IR measurement). Sasaki and his coworkers investigated a self-assembled monolayer (SAM) of an oxo-centered tri-ruthenium cluster $[Ru_3(\mu_3\text{-}O)(\mu\text{-}CH_3COO)_6(CO)(L_1)(L_2)]$ ($L_1 = [(NC_5H_4)CH_2NHC(O)(CH_2)_{10}S\text{-}]_2$, L_2 = 4-methylpyridine) on gold electrode surface by *in situ* IR measurement.[269] The *in situ* IR characterization gives valuable information for CO ligand the cluster during the potential-dependent ligand exchange reaction where the IR frequency and peak shape for CO-ligand largely change with potential and it is easy to distinguish the contribution from sample and reference spectra. However, the analysis is facing a difficulty to understand the potential dependence of six acetate groups in the cluster. The symmetric and asymmetric OCO stretching modes change with oxidation states of central Ru ions in quite complicated way. It is almost impossible to separate the spectral contribution from sample and reference IR spectra in comparison with CO ligand. Thus, *in situ* SFG measurements were carried out to determine the absolute spectra for the acetate group in the SAM. Figure. 18 shows SFG spectra (1700～1500 cm^{-1}) for one-electron redox process between $[(Ru^{II}-CO)Ru^{III}Ru^{III}]^0$ (+0.3 V) and $[(Ru^{III}-CO)Ru^{III}Ru^{III}]^{+1}$ (+0.9 V). The SFG spectrum of the ν_{as}(OCO) at +0.3 V gives two peaks at 1615 and 1573 cm^{-1}. As the potential is stepped to +0.9 V, the peak at 1615 cm^{-1} decreases to nearly half intensity and the peak at 1573 cm^{-1} almost disappears. Based on the spectral changes here, we can quantitatively explain the *in situ* IR spectra namely one of ν_{as}(OCO) modes becomes weaker and another one disappears after one-electron oxidation at +0.9 V.[269]

As a typical application of *in situ* SFG measurement on electrode and solution interface, Fig. 19 shows *in situ* SFG spectra reported by Gewirth *et al.* for adsorption of benzotriazole (BTAH) on Cu(100) and Cu(111) electrode surface in acidic solution, which has been used as copper corrosion inhibitor.[270] Even 75 mM BTAH molecules are included in the solution, potential-dependent SFG measurement can distinguish surface adsorbed species form solution species and exhibits that BTAH is adsorbed because the adsorbed molecule is the benzotriazole anion (BTA^-) at all potentials investigated. It is found that an ordered BTA^- adlayer is formed on Cu(100) than Cu(111), especially on the negative potential region. Based on the information, they proposed BTA^- coordinated to the surface and Cu^+ ions in solution. This information is expected to understand the difference in the corrosion inhibition for two copper surfaces.[270]

It should be mentioned here, however, although SFG measurements have been applied in many electrochemical systems such as adsorption of CO, CN^-, SCN^-, H and water molecules on various electrode surfaces,[39-41] most of these studies, for example, CO adsorption, can be also obtained by *in situ* IR measurement using commercially available FTIR spectrometer. The SFG measurements fully utilizing its superior advantages are still very limited. One of technical problems is that *in situ* SFG measurements are still using a spectroscopic cell with thin-layer geometry similar to that used *in situ* IR measurement. This structure can largely affect the mass transport and potential distribution in the thin layer and can generate a serious problem for a long term experi-

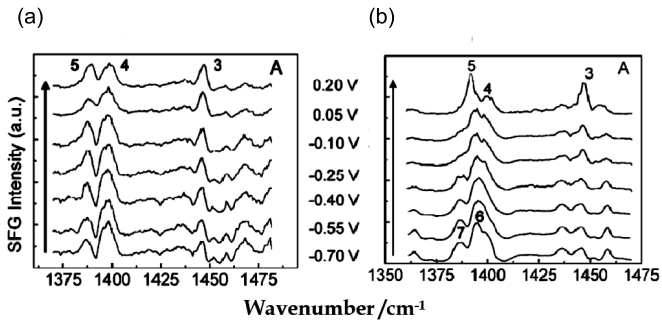

Fig. 19 Potential-dependent SFG spectrum obtained from (a) Cu(100) and (b) Cu(111) electrode in 0.1 M H_2SO_4 and 75 mM BTAH solution at the indicated potentials in the anodic scan. Arrows indicate scan direction. The spectra are offset for clarity. Reprinted with permission from Ref. 270, Copyright American Chemical Society (2004).

ment.[271-273] On the other hand, the thin-layer structure of electrolyte solution can strongly absorb IR light and will make a difficulty to study the structure of the water molecules on the electrode surface.[274] Total internal reflection mode with Kretschmann geometry may be one promising way to overcome the problem.

Although many issues need to be improved, we believe that SFG and SHG techniques will provide us valuable structural information on the electrode surface which is impossible to be obtained by conventional spectroscopy methods.

7 Summary & Outlook

In this review, we summarized recent advances in *in situ* surface characterization techniques combined with single crystal electrochemistry. The understanding of electrolyte-electrode interface at atomic and/or molecular level has made considerable progress by the use of those *in situ* techniques in the past decade, and the results have provided many knowledge for various electrode reaction processes and new surface design. In the near future, for example, to precisely understand various electrode reaction processes in room temperature ionic liquids (RTILs) which are promising electrolyte for the control of various electrochemical reaction on electrode surfaces[275] at atomic and/or molecular level, *in situ* techniques will provide us new information. Surface electrochemistry using single crystal electrodes will play an important role in the understanding of electrochemical reaction process.

Acknowledgement

This work is partly supported by Grant-in-Aid from the Ministry of Education, Culture, Sports, Science, and Technology, Japan.

References

1) A. J. Bard and R. M. Crooks, *Langmuir,* **22**, 10297 (2006), and see articles published in the same special issue on Electrochemistry from pp. 10299-10875.
2) G. Jerkiewicz, *Solid-Liquid Electrochemical Interfaces (ACS Symposium Series 656)*, G. Jerkiewicz, (Eds. M. P. Soriaga, K. Uosaki, and A. Wieckowski), American Chemical Society, Washington DC, p. 1 (1997).
3) K. Itaya, *Prog. Surf. Sci.,* **58**, 121 (1998).
4) A. Wieckowski, *Interfacial Electrochemistry*, Marcel Dekker, Inc, New York (1999).
5) J. Clavilier, R. Faure, G. Guinet, and R. Durand, *J. Electroanal. Chem.,* **107**, 205 (1980).
6) J. Clavilier, *J. Electroanal. Chem.,* **107**, 205 (1980).
7) A. Hamelin, *Modern Aspects of Electrochemistry*, (Eds. B. E. Conway, R. E. White and J.O'M. Bockris,) No.16, Plenum Press, New York, Chap. 1 (1985).
8) A. Hamelin, *J. Electroanal. Chem.,* **407**, 1 (1996).
9) S. Motoo and N. Furuya, *J. Electroanal. Chem.,* **167**, 309 (1984).
10) K. Sashikata, N. Furuya, and K. Itaya, *J. Vac. Sci. Technol. B,* **9**, 457 (1991).
11) R. J. Nichols, *Adsorption of molecules at metal electrodes*, (Eds. J. Lipkowski and P. N. Ross), VCH, New York, p. 347 (1992).
12) T. Iwasita and F. C. Nart, *Prog. Surf. Sci.,* **55**, 271 (1997).
13) H. D. Abruña, *Modern Techniques for In-Situ Interface Characterization in Electrochemical Interfaces*, VCH, New York (1991).
14) J. Lipkowski and P. N. Ross, *Structure of Electrified Interfaces*, VCH, New York (1993).
15) K. Itaya and E. Tomita, *Surf. Sci.,* **201**, L507 (1988).
16) D. M. Kolb, *Prog. Surf. Sci.,* **51**, 109 (1996).
17) A. A. Gewirth and B. K. Niece, *Chem. Rev.,* **97**, 1129 (1997).
18) O. M. Magnussen, *Chem. Rev.,* **102**, 679 (2002).
19) K. Itaya, *Electrochemistry,* **74**, 19 (2006).
20) D. Wang and L.-J. Wan, *J. Phys. Chem. C,* **111**, 16109 (2007).
21) S. Chiang, *Chem. Rev.,* **97**, 1083 (1997).
22) S. De Feyter and F. C. De Schryver, *Chem. Soc. Rev.,* **32**, 139 (2003).
23) M. Hepel, K. Kanige, and S. Bruckenstein, *J. Electroanal. Chem.,* **266**, 409 (1989).
24) A. J. Kelly and N. Oyama, *J. Phys. Chem.,* **95**, 9579 (1991).
25) K. Shimazu and H. Kita, *J. Electroanal. Chem.,* **341**, 361 (1992).
26) K. Shimazu, I. Yagi, Y. Sato, and K. Uosaki, *Langmuir,* **8**, 1385 (1992).
27) T. Tatsuma, S. Kikuyama, and N. Oyama, *J. Phys. Chem.,* **97**, 12067 (1993).
28) H. Uchida, N. Ikeda, and M. Watanabe, *J. Electroanal. Chem.,* **424**, 5 (1997).
29) Z. Q. Tian, B. Ren, J. Li, and Z. Yang, *Chem. Commun.*, **2007**, 3514.
30) K. Ataka, T. Yotsuyanagi, and M. Osawa, *J. Phys. Chem.,* **100**, 10664 (1996).
31) M. Osawa, *Bull. Chem. Soc. Jpn.,* **70**, 2861(1997).
32) K. Ataka and M. Osawa, *Langmuir,* **14**, 951 (1998).
33) B. Pettinger, J. Lipkowski, S. Mirwald, and A. Friedrich, *J. Electroanal. Chem.,* **329**, 289 (1992).
34) G. L. Richmond, J. M. Robinson, and V. L. Shannon, *Prog. Surf. Sci.,* **28**, 1 (1988).
35) R. M. Corn and D. A. Higgins, *Chem. Rev.,* **94**, 107 (1994).
36) I. Yagi, J. M. Lantz, S. Nakabayashi, R. M. Corn, and K. Uosaki, *J. Electroanal. Chem.,* **401**, 95 (1996).
37) P. Miranda and Y. R. Shen, *J. Phys. Chem. B,* **103**, 3292 (1999).
38) G. L. Richmond, *Chem. Rev.,* **102**, 2693 (2002).
39) C. D. Bain, *J. Chem. Soc. Faraday Trans.,* **91**, 1281 (1995).
40) A. Tadjeddine and A. Peremans, *Spectroscopy for Surface Science*, (Eds. R. J. H. Clark and R. E. Hester), Wiley & Sons Ltd, Chichester, UK, p. 159 (1998).
41) S. Ye and K. Uosaki, *Encyclopedia of Electrochemistry*, (Ed. A. J. Bard), Vol. 10, Wiley-VCH, Weinheim, p. 513 (2007).
42) Y. R. Shen and V. Ostroverkhov, *Chem. Rev.,* **106**, 1140 (2006).
43) Z. D. Schultz, S. K. Shaw, and A. A. Gewirth, *J. Am. Chem. Soc.,* **127**, 15916 (2005).
44) S. Baldelli, *Acc. Chem. Res.,* **41**, 421 (2008).
45) J. Wang, B. M. Ocko, A. J. Davenport, and H. S. Isaacs, *Phys. Rev. B,* **46**, 10321 (1992).
46) J. Wang, A. J. Davenport, H. S. Isaacs, and B. M. Ocko,

Science, **255**, 1416 (1992).
47) B. M. Ocko, G. M. Watson, and J. Wang, *J. Phys. Chem.,* **98**, 897 (1994).
48) E. Herrero, L. J. Buller, and H. D. Abruña, *Chem. Rev.,* **101**, 1897 (2001).
49) A. Ulman, *Introduction to Ultrathin Organic Films*, Academic Press, Boston (1991).
50) A. Ulman, *Chem. Rev.,* **96**, 1533 (1996).
51) G. E. Poirier, *Chem. Rev.,* **97**, 1117 (1997).
52) J. C. Love, L. A. Estroff, J. K. Kriebel, R. G. Nuzzo, and G. M. Whitesides, *Chem. Rev.,* **105**, 1103 (2005).
53) S. Yoshimoto, *Bull. Chem. Soc. Jpn.,* **79**, 1167 (2006).
54) S. Yoshimoto and K. Itaya, *J. Porphyrins Phthalocyanines,* **11**, 313 (2007).
55) S. Yoshimoto and K. Itaya, *Bottom-up Nanofabrication: Supramolecules, Self-Assemblies, and Organized Films*, (Eds. K. Ariga and H. S. Nalwa), American Scientific Publishers, California, Chap. 71 (2008).
56) S. Yoshimoto, S. Sugawara, and K. Itaya, *Electrochemistry,* **74**, 175 (2006).
57) S. Yoshimoto, E. Tsutsumi, R. Narita, K. Fujiwara, M. Murata, Y. Murata, K. Komatsu, O. Ito, and K. Itaya, *J. Am. Chem. Soc.,* **129**, 4366 (2007).
58) S. Yoshimoto, Y. Honda, O. Ito, and K. Itaya, *J. Am. Chem. Soc.,* **130**, 1085 (2008).
59) S. Yoshimoto and T. Sawaguchi, *J. Am. Chem. Soc.,* **130**, 15944 (2008).
60) K. Kaji, S.-L.Yau, and K. Itaya, *J. Appl. Phys.,* **78**, 5727 (1995).
61) H. Yao, S.-L. Yau, and K. Itaya, *Appl. Phys. Lett.,* **68**, 1473 (1996).
62) J. Inukai, K. Ito, and K. Itaya, *Electrochemistry,* **67**, 1126 (1999).
63) J. E. Anthony, *Angew. Chem. Int. Ed.,* **47**, 452 (2008).
64) H. Schwertfeger, A. A. Fokin, and P. R. Schreiner, *Angew. Chem. Int. Ed.,* **47**, 1022 (2008).
65) B. Ulgut and H. D. Abruña, *Chem. Rev.,* **108**, 2721 (2008) and references therein.
66) R. Feidenhans'l, *Surf. Sci. Rep.,* **10**, 105 (1989).
67) I. K. Robinson and D. J. Tweet, *Rep. Prog. Phys.,* **55**, 599 (1992).
68) M. F. Toney and O. R. Melroy, *Electrochemical Interface: Modern Techniques for In Situ Interfacial Characterization*, (Ed. H. D. Abruña), VCH Publishers, Inc., New York, Chap. 2 (1991).
69) M. F. Toney and J. McBreen, *Interface*, The Electrochemical Society, Spring, Vol. 2, pp. 22-31 (1993).
70) M. F. Toney, *Synchrotron Techniques in Interfacial Electrochemistry, NATO ASI Series*, (Eds. C. A. Melendres and A. Tadjeddine), Kluwer Academic, Boston (1994).
71) B. M. Ocko and J. Wang, *Synchrotron Techniques in Interfacial Electrochemistry, NATO ASI Series*, (Eds. C. A. Melendres and A. Tadjeddine), Kluwer Academic, Boston (1994).
72) J. Wang, G. M. Watson, and B. M. Ocko, *Physica A,* **200**, 679 (1993).
73) B. M. Ocko, J. Wang, A. Davenport, and H. Isaacs, *Phys. Rev. Lett.,* **65**, 1466 (1990).
74) B. M. Ocko, G. Helgesen, B. Schardt, J. Wang, and A. Hamelin, *Phys. Rev. Lett.,* **69**, 3350 (1992).
75) M. F. Toney, J. G. Gordon, M. G. Sammant, G. L. Borges, D. G. Wiesler, D. Yee, and L. B. Sorensen, *Langmuir,* **7**, 796 (1991).
76) M. F. Toney, J. G. Gordon, M. G. Sammant, G. L. Borges, O. R. Melroy, D. Yee, and L. B. Sorensen, *Phys. Rev. B,* **45**, 9362 (1992).
77) G. Scherb, A. Kazimirov, J. Zegenhagen, T. Schultz, R. Feidenhans'l, and B. O. Fimland, *Appl. Phys. Lett.,* **71**, 2990 (1997).
78) C. Aruta, F. Ricci, G. Balestrino, S. Lavanga, P. G. Medaglia, P. Orgiani, A. Tebano, and J. Zegenhagen, *Phys. Rev. B,* **65**, 195408 (2002).
79) A. H. Ayyad, J. Stettner, and O. M. Mugnussen, *Phys. Rev. Lett.,* **94**, 066106 (2005).
80) K. Krug, J. Stettner, and O. M. Magnussen, *Phys. Rev. Lett.,* **96**, 246101 (2006).
81) M. Takahasi, Y. Hayashi, J. Mizuki, K. Tamura, T. Kondo, H. Naohara, and K. Uosaki, *Surf. Sci.,* **461**, 213 (2000).
82) K. Uosaki, S. Ye, T. Kondo, and H. Naohara, *Thin Solid Films: Preparation, Characterization, Applications*, (Eds. M. P. Soriaga, J. Stickney, L. A. Bottomley, and Y.-G. Kim), Kluwer Academic/Plenum Publishers, New York, pp. 17-35 (2002).
83) T. Kondo, J. Morita, M. Okamura, T. Saito, and K. Uosaki, *J. Electroanal. Chem.,* **532**, 201 (2002).
84) T. Kondo, K. Tamura, M. Takahasi, J. Mizuki, and K. Uosaki, *Electrochim. Acta,* **47**, 3075 (2002).
85) T. Kondo, J. Morita, K. Hanaoka, S. Takakusagi, K. Tamura, M. Takahasi, J. Mizuki, and K. Uosaki, *J. Phys. Chem. C,* **111**, 13197 (2007).
86) A. Hamelin, *J. Electroanal. Chem.,* **142**, 229 (1992).
87) X. Gao, A. Hamelin, and M. J. Weaver, *J. Chem. Phys.,* **95**, 6993 (1991).
88) M. S. Zei, G. Lehmpfuhl, and D. M. Kolb, *Surf. Sci.,* **221**, 23 (1989).
89) A. Cuesta, M. Kleinert, and D. M. Kolb, *Phys. Chem. Chem. Phys.,* **2**, 5684 (2000).
90) K. Sato, S. Yoshimoto, J. Inukai, and K. Itaya, *Electrochem. Commun.,* **8**, 725 (2006).
91) A. Angerstein-Kozlowska, B. E. Conway, A. Hamelin, and L. Stoicoviciu, *Electrochim. Acta,* **31**, 1051 (1986).
92) A. Angerstein-Kozlowska, B. E. Conway, A. Hamelin, and L. Stoicoviciu, *J. Electroanal. Chem.,* **228**, 429 (1987).
93) R. Woods, *Electroanalytical Chemistry: A Series of Advances*, (Ed. A. J. Bard), Marcel Dekker, New York (1988).
94) C. M. Vitus and A. J. Davenport, *J. Electrochem. Soc.,* **141**, 1291 (1994).
95) D. M. Kolb, *Prof. Surf. Sci.,* **51**, 109 (1996).
96) K. M. Robinson, I. K. Robinson, and W. E. O'Grady, *Surf. Sci.,* **262**, 387 (1992).
97) S. Motoo and N. Furuya, *Ber. Bunsenges. Chem. Phys.,* **91**, 457 (1987).
98) N. Furuya and S. Koide, *Surf. Sci.,* **220**, 18 (1989).
99) N. M. Marković, N. S. Marinković, and R. R. Ažić, *J. Electroanal. Chem.,* **241**, 309 (1988).
100) J. Clavilier, K. El Achi, and A. Rodes, *J. Electroanal. Chem.* **272**, 253 (1989).
101) A. Rodes, K. El Achi, M. A. Zamakhchari, and J. Clavilier, *J. Electroanal. Chem.,* **284**, 245 (1990).
102) P. N. Ross, *J. Chim. Phys.,* **88**, 1353 (1991).
103) J. M. Feliu, A. Rodes, J. M. Orts, and J. Clavilier, *Polish*

J. Phys. Chem., **68**, 1575 (1994).
104) J. M. Feliu, A. Fernindez-Vega, A. Aldaz, and J. Clavilier, *J. Electroanal. Chem.,* **256**, 149 (1988).
105) J. Clavilier, J. M. Feliu, and A. Aldaz, *J. Electroanal. Chem.,* **243**, 419 (1988).
106) G. Gomez, M. J. Llorca, J. M. Feliu, and A. Aldaz, *J. Electroanal. Chem.,* **340**, 349 (1992).
107) P. Rodrlguez, E. Herrero, J. Solla-Gullon, F. J. Vidal-Iglesias, A. Aldaz, and J. M. Feliu, *Electrochim. Acta,* **50**, 4308 (2005).
108) N. Furuya and S. Koide, *Surf. Sci.,* **226**, 221 (1990).
109) M. Wasberg, M. Hourani, and A. Wieckowski, *J. Electroanal. Chem.,* **278**, 425 (1990).
110) T. H. M. Housmans, J. M. Feliu, and M. T. M. Koper, *J. Electroanal. Chem.,* **572**, 79 (2004).
111) N. Hoshi, K. Kagaya, and Y. Hori, *J. Electroanal. Chem.,* **485**, 55 (2000).
112) N. Hoshi, M. Kuroda, and Y. Hori, *J. Electroanal. Chem.,* **521**, 155 (2002).
113) K. Sashikata, Y. Matsui, K. Itaya, and M. P. Soriaga, *J. Phys. Chem.,* **100**, 20027 (1996).
114) S. Tanaka, S.-L. Yau, and K. Itaya, *J. Electroanal. Chem.,* **396**, 125 (1995).
115) C. M. Vitus, S.-C. Chang, B. C. Schardt, and M. J. Weaver, *J. Phys. Chem.,* **95**, 7559 (1991).
116) M. Wakisaka, T. Ohkanda, T. Yoneyama, H. Uchida, and M. Watanabe, *Chem. Commun*., **2005**, 2710.
117) I. M. Tidswell, N. M. Markovic, and P. N. Ross, *J. Electroanal. Chem.,* **376**, 119 (1994).
118) I. M. Tidswell, N. M. Markovic, and P. N. Ross, *Phys. Rev. Lett.,* **71**, 1601 (1993).
119) C. A. Lucas, N. M. Markovic, and P. N. Ross, *Phys. Rev. Lett.,* **77**, 4922 (1996).
120) N. M. Markovic, B. N. Grgur, C. A. Lucas, and P. N. Ross, *Surf. Sci.,* **384**, L805 (1997).
121) D. W. Blakely and G. A. Somorjai, *Surf. Sci.,* **65**, 419 (1977).
122) A. Nakahara, M. Nakamura, K. Sumitani, O. Sakata, and N. Hoshi, *Langmuir,* **23**, 10879 (2007).
123) N. Hoshi, A. Nakahara, M. Nakamura, K. Sumitani, and O. Sakata, *Electrochim. Acta,* **53**, 6070 (2008).
124) N. M. Marković, B. N. Grugur, and P. N. Ross, *J. Phys. Chem.,* **101**, 5405 (1997).
125) N. M. Marković and P. N. Ross, *Surf. Sci. Rep.,* **45**, 117 (2002).
126) R. J. Nichols and A. Bewick, *J. Electroanal. Chem.,* **243**, 445 (1988).
127) K. Kunimatsu, H. Uchida, M. Osawa, and M. Watanabe, *J. Electroanal. Chem.,* **587**, 299 (2006).
128) K. Kunimatsu, T. Senzaki, G. Samjeske, M. Tsushima, and M. Osawa, *Electrochim. Acta,* **52**, 5715 (2007).
129) D. Strmcnik, D. Tripkovic, D. van der Vliet, V. Stamenkovic, and N. M. Marković, *Electrochem. Commun.,* **10**, 1602 (2008).
130) R. F. Mann, J. C. Amphlett, B. A. Peppley, and C. P. Thurgood, *J. Power Sources,* **163**, 679 (2007).
131) N. Hoshi, M. Nakamura, Y. Asaumi, and K. Mikita, to be submitted to *Electrochem. Commun.*
132) M. Otani, I. Hamada, O. Sugino, Y. Morikawa, Y. Okamoto, and T. Ikeshoji, *J. Phys. Soc. Jpn.,* **77**, 024872 (2008).
133) N. M. Marković, R. R. Ažić, B. D. Cahan, and E. Yeager, *J. Electroanal. Chem.,* **377**, 249 (1994).
134) N. M. Marković, H. A. Gasteiger, and P. N. Ross, *J. Phys. Chem.,* **99**, 3411 (1995).
135) N. M. Marković, H. Gasteiger, and P. N. Ross, *J. Electrochem. Soc.,* **144**, 1591 (1997).
136) B. N. Grgur, N. M. Marković, and P. N. Ross, Can. *J. Chem.,* **75**, 1465 (1997).
137) F. El Kadiri, R. Faure, and R. Durand, *J. Electroanal. Chem.,* **301**, 177 (1991).
138) H. Kita, H.-W. Lei, and Y. Gao, *J. Electroanal. Chem.,* **379**, 407 (1994).
139) M. D. Macia, J. M. Campina, E. Herrero, and J. M. Feliu, *J. Electroanal. Chem.,* **564**, 141 (2004).
140) N. Hoshi, A. Sakurada, S. Nakamura, S. Teruya, O. Koga, and Y. Hori, *J. Phys. Chem. B,* **106**, 1985 (2002).
141) P. W. Faguy, N. M. Marković, R. R Ažić, C. A. Fierro, and E. Yeager, *J. Electroanal. Chem.,* **289**, 245 (1990).
142) R. J. Nichols, *Adsorption of Molecules at Metal Electrodes*, (Eds. J. L. Lipkowski, and P. N. Ross, Jr.), VCH, New York, Chap. 7 (1991).
143) Y. Sawatari, J. Inukai, and M. Ito, *J. Electron Spectrosc.,* **64/65**, 515 (1993).
144) F. C. Nart, T. Iwasita, and M. Weber, *Electrochim. Acta,* **39**, 961 (1994).
145) S. Thomas, Y.-E. Sung, H. S. Kim, and A. Wieckowski, *J. Phys. Chem.,* **100**, 11726 (1996).
146) P. W. Faguy, N. S. Marinković, and R. R. Ažić, *Langmuir,* **12**, 243 (1996).
147) P. W. Faguy, N. S. Marinković, and R. R. Ažić, *J. Electroanal. Chem.,* **407**, 209 (1996).
148) F. C. Nart, T. Iwasita, and M. Weber, *Electrochim. Acta,* **39**, 2093 (1994).
149) T. Iwasita, F. C. Nart, A. Rodes, E. Pastor, and M. Weber, *Electrochim. Acta,* **40**, 53 (1995).
150) M. D. Macia, J. M. Campina, E. Herrero, and J. M. Feliu, *J. Electroanal. Chem.,* **564**, 141 (2004).
151) A. Kuzume, E. Herrero, and J. M. Feliu, *J. Electroanal. Chem.,* **599**, 333 (2007).
152) N. Hoshi, M. Nakamura, S. Kondo, and N. Maki, to be submitted to *Electrochem. Commun.*
153) F. Kitamura, M. Takeda, M. Takahashi, and M. Ito, *Chem. Phys. Lett.,* **142**, 318 (1987).
154) L.-W.-H. Leung, A. Wieckowski, and M. J. Weaver, *J. Phys. Chem.,* **92**, 6985 (1988).
155) N. Furuya, S. Motoo, and K. Kunimatsu, *J. Electroanal. Chem.,* **239**, 347 (1988).
156) F. Kitamura, M. Takahashi, and M. Ito, *J. Phys. Chem.,* **92**, 3320 (1988).
157) S. Watanabe, Y. Kinomoto, F. Kitamura, M. Takahashi, and M. Ito, *J. Electron. Spectrsc. Rel. Phenom.,* **54/55**, 1205 (1990).
158) S.-C. Chung and M. J. Weaver, *J. Phys. Chem.,* **94**, 5095 (1990).
159) S.-C. Chung and M. J. Weaver, *Surf. Sci.,* **230**, 222 (1990).
160) I. Villegas and M. J. Weaver, *J. Chem. Phys.,* **101**, 1648 (1994).
161) S. Watanabe, J. Inukai, and M. Ito, *Surf. Sci.,* **293**, 1 (1993).
162) A. Rodes, R. Gómez, J. M. Feliu, and M. J. Weaver, *Langmuir,* **16**, 811 (2000).
163) N. P. Lebedeva, A. Rodes, J. M. Feliu, M. T. M. Koper, and R. A. van Santen, *J. Phys. Chem. B,* **106**, 12938 (2002).

164) N. Hoshi, M. Tanizaki, O. Koga, and Y. Hori, *Chem. Phys. Lett.,* **336**, 13 (2001).
165) C. S. Kim and C. Korzeniewski, *Anal. Chem.,* **69**, 2349 (1997).
166) C. S. Kim, W. J. Tornquist, and C. Korzeniewski, *J. Phys. Chem.,* **97**, 6484 (1993).
167) C. S. Kim, C. Korzeniewski, and W. J. Tornquist, *J. Chem. Phys.,* **100**, 628 (1994).
168) K. Mikita, M. Nakamura, and N. Hoshi, *Langmuir,* **23**, 9092 (2007).
169) N. P. Lebedeva, M. T. M. Koper, E. Herrero, J. M. Feliu, and R. A. van Santen, *J. Electroanal. Chem.,* **487**, 37 (2000).
170) N. Hoshi, *Hyomen,* **43**, 8 (2005).
171) S. Gilman, *J. Phys. Chem.,* **68**, 70 (1964).
172) R. Parsons and T. van der Noot, *J. Electroanal. Chem.,* **257**, 9 (1988).
173) M. T. M. Koper, A. P. J. Jansen, R. A. van Santen, J. J. Lukkien, and P. A. J. Hilbers, *J. Chem. Phys.,* **109**, 6051 (1998).
174) T. Biegler, *Aus. J. Chem.,* **26**, 2571 (1973).
175) E. Hererro, K. Franaszuczuk, and A. Wieckowski, *J. Phys. Chem.,* **98**, 5074 (1994).
176) H. Shiroishi, Y. Ayato, K. Kunimatsu, and T. Okada, *J. Electroanal. Chem.,* **581**, 132 (2005).
177) K. Kunimatsu, T. Sato, H. Uchida, and M. Watanabe, *Langmuir,* **24**, 3590 (2008).
178) K. Yoshioka, F. Kitamura, M. Takeda, M. Takahashi, and M. Ito, *Surf. Sci.,* **227**, 90 (1990).
179) S. Zou, R. Gómez, and M. J. Weaver, *J. Electroanal. Chem.,* **474**, 155 (1999).
180) S. Zou, R. Gómez, and M. J. Weaver, *Langmuir,* **15**, 2931 (1999).
181) S. Zou, R. Gómez, and M. J. Weaver, *Surf. Sci.,* **399**, 270 (1998).
182) N. Hoshi, O. Koga, Y. Hori, and T. Ogawa, *J. Electroanal. Chem.,* **587**, 79 (2006).
183) T. H. M. Housmans and M. T. M. Koper, *J. Electroanal. Chem.,* **575**, 39 (2005).
184) T. H. M. Housmans, and M. T. M. Koper, *Electrochem. Commun.,* **7**, 581 (2005).
185) B. Beden, A. Bewick, and C. Lamy, *J. Electroanal. Chem.,* **148**, 147 (1983).
186) K. Kunimatsu, *J. Electroanal. Chem.,* **213**, 149 (1986).
187) S. G. Sun and J. Clavilier, *J. Electroanal. Chem.,* **240**, 147 (1988).
188) A. Miki, S. Ye, and M. Osawa, *Chem. Commun.*, **2002**, 1500.
189) G. Samjeské, A. Miki, S. Ye, A. Yamakata, Y. Mukouyama, H. Okamoto, and M. Osawa, *J. Phys. Chem. B,* **109**, 23509 (2005).
190) G. Samjeské, A. Miki, S. Ye, and M. Osawa, *J. Phys. Chem. B,* **110**, 16559 (2006).
191) R. R. Adžić, A. V. Tripković, and W. E. O'Grady, *Nature,* **296**, 137 (1982).
192) S. Motoo and N. Furuya, *J. Electroanal. Chem.,* **184**, 303 (1985).
193) S. G. Sun and J. Clavilier, *J. Electroanal. Chem.,* **199**, 471 (1986).
194) C. Lamy and J. M. Légar, *J. Chim. Phys.,* **88**, 1649 (1991).
195) S. G. Sun, Y. Lin, N. H. Li, and J. Q. Mu, *J. Electroanal. Chem.,* **370**, 273 (1994).
196) K. Nishimura, K. Kunimatsu, K. Machida, and M. Enyo, *J. Electroanal. Chem.,* **260**, 181 (1989).
197) S. Pronkin, M. Hara, and T. Wandlowski, *Russian J. Electrochem.,* **42**, 1177 (2006).
198) H. Miyake, T. Okada, G. Samjeské, and M. Osawa, *Phys. Chem. Chem. Phys.,* **10**, 3662 (2008).
199) M. Baldauf and D, M. Kolb, *J. Phys. Chem.,* **100**, 11375 (1996).
200) N. Hoshi, K. Kida, M. Nakamura, M. Nakada, and K. Osada, *J. Phys. Chem. B,* **110**, 12480 (2006).
201) N. Hoshi, M. Kuroda, O. Koga, and Y. Hori, *J. Phys. Chem. B,* **106**, 9107 (2002).
202) N. Hoshi, M. Kuroda, T. Ogawa, O. Koga, and Y. Hori, *Langmuir,* **20**, 5066 (2004).
203) N. Hoshi, M. Nakamura, and K. Kida, *Electrochem. Commun.,* **9**, 279 (2007).
204) Y. X. Chen, A. Miki, S. Ye, and M. Osawa, *J. Am. Chem. Soc.,* **125**, 3680 (2003).
205) M. Nakamura, K. Shibutani, and N. Hoshi, *ChemPhysChem.,* **8**, 1846 (2007).
206) J. Clavilier, C. Lamy, and J. M. Leger, *J. Electroanal. Chem.,* **125**, 249 (1982).
207) E. Herrero, K. Franaszczuk, and A. Wieckowski, *J. Phys. Chem.,* **98**, 5074 (1994).
208) C. Lamy and J. M. Legar, *J. Electroanal. Chem.,* **135**, 321 (1982).
209) A. V. Tripković, K. Dj. Popović, J. D. Momčilović, and D. M. Dražić, *J. Electroanal. Chem.,* **418**, 9 (1996).
210) S. G. Sun and J. Clavilier, *J. Electroanal. Chem.,* **236**, 95 (1987).
211) T. H. M. Housmans and M. T. M. Koper, *J. Phys. Chem.,* **107**, 8557 (2003).
212) I. T. Bae, X. Xing, C. C. Liu, and E. Yeager, *J. Electroanal. Chem.,* **284**, 335 (1990).
213) I. T. Bae, E. Yeager, X. Xing, and C. C. Liu, *J. Electroanal. Chem.,* **309**, 131 (1991).
214) B. Beden, F. Largeaud K. B. Kokoh, and C. Lamy, *Electrochim. Acta,* **41**, 701 (1996).
215) K. Dj. Popović, N. M. Marković, A. V. Tripković, and R. R Ažić, *J. Electroanal. Chem.,* **295**, 79 (1990).
216) K. Dj. Popović, N. M. Marković, A. V. Tripković, and R. R Ažić, *J. Electroanal. Chem.,* **313**, 181 (1990).
217) M. J. Llorca, J. M. Feliu, A. Aldaz, J. Clavilier and A. Rodes, *J. Electroanal. Chem.,* **316**, 175 (1991).
218) A. Ahmadi, G. Attard, J. M. Feliu, and A. Rodes, *Langmuir,* **15**, 2420 (1999).
219) G. A. Attard, A. Ahmadi, J. M. Feliu, A. Rodes, E. Herrero, S. Blais, and G. Jerkiewicz, *J. Phys. Chem. B,* **103**, 1381(1999).
220) G. A. Attard, *J. Phys. Chem. B,* **105**, 3158 (2001).
221) G. A. Attard, C. Harris, E. Herrero, and J. M. Feliu, *Faraday Discuss.,* **121**, 253 (2002).
222) O. A. Hazzazil, G. A. Attard, and P. B. Wells, *J. Mol. Cat. A,* **216**, 247 (2004).
223) T. S. Ahmadi, Z. L. Wang, T. C. Green, A. Henglein, and M. A. El-Sayed, *Science,* **272**, 1924, (1996).
224) T. Teranishi, R. Kurita, and M. Miyake, *J. Inorg. Organometallic Polymers,* **10**, 145 (2000).
225) M. Yamada, S. Kon, and M. Miyake, *Chem. Lett.,* **34**, 1050 (2005).
226) N. Tian, Z. Y. Zou, S. G. Sun, Y. Ding, and Z. L. Wan, *Science,* **316**, 732 (2007).
227) M. Inaba, M Ando, A. Hatanaka, A. Nomoto, K.

Matsuzawa, A. Tasaka, T. Kinumoto, Y. Iriyama, and Z. Ogumi, *Electrochim. Acta,* **52**, 1632 (2006).
228) J. Solla-Gullon, P. Rodriguez, E. Herrero, A. Aldaz, and J. M. Feliu, *Phys. Chem. Chem. Phys.,* **10**, 1359 (2008).
229) M. Labayen, C. Ramirez, W. Schattke, and O. M. Magnussen, *Nature Mater.,* **2**, 783 (2003).
230) M. A. van Hove, R. J. Koestmer, P. C. Stair, J. P. Biberian, L. L. Kesmodel, I. Bartos, and G. A. Somorjai, *Surf. Sci.,* **103**, 189 (1981).
231) J. Clavilier, A. Rodes, K. El. Achi, and M. A. Zamakhchari, *J. Chim. Phys.,* **88**, 1291 (1991).
232) K. Sashikata, T. Sugata, M. Sugimasa, and K. Itaya, *Langmuir,* **14**, 2896 (1998).
233) M. Wakisaka, M. Sugimasa, J. Inukai, and K. Itaya, *J. Electrochem. Soc.,* **150**, E81 (2003).
234) O. M. Magnussen, L. Zitzler, B. Gleich, M. R. Vogt, and R. J. Behm, *Electrochim. Acta,* **46**, 3725 (2001).
235) O. M. Magnussen, W. Polewska, L. Zitzler, and R. J. Behm, *Faraday Discuss.,* **121**, 43 (2002).
236) S. Strbac, C. M. Johnston, G. Q. Lu, A. Crown, and A. Wieckowski, *Surf. Sci.* **573**, 80 (2004).
237) S. Strbac, C. M. Johnston, and A. Wieckowski, *Russian J. Electrochem.,* **42**, 1244 (2006).
238) C. Jung, B. Ku, J. Kim, and C. K. Rhee, *Chem. Commun.*, **2006**, 2191.
239) A. Miki, S. Ye, T. Senzaki, and M. Osawa, *J. Electroanal. Chem.,* **563**, 23 (2004).
240) M. Osawa, *Diffraction and Spectroscopic Methods in Electrochemistry* (Advances in Electrochemical Science and Engineering, Vol. 9) (Eds. R. C. Alkire, D. M. Kolb, J. Lipkowski, and P. H. Ross), Wiley-VCH, Weinhiem, Chap 8 (2006).
241) G. Samjeské and M. Osawa, *Angew. Chem. Int. Ed.,* **44**, 5694 (2005).
242) G. Samjeské, A. Miki, and M. Osawa, *J. Phys. Chem. C,* **111**, 15074 (2007).
243) M. Osawa, K. Yoshii, K. Ataka, and T. Yotsuyanagi, *Langmuir,* **10**, 640 (1994).
244) H. Noda, K. Ataka, L.-J. Wan, and M. Osawa, *Surf. Sci.,* **427-428**, 190 (1999).
245) A. Rodes, J. M. Orts, J. M. Rerez, J. M. Feliu, and A. Aldaz, *Electrochem. Commun.,* **5**, 56 (2003).
246) H. Noda, L.-J. Wan, and M. Osawa, *Phys. Chem. Chem. Phys.,* **3**, 3336 (2001).
247) J. F. Smalley, C. V. Krishnan, M. Goldman, S. W. Feldberg, and I. Ruzic, *J. Electroanal. Chem.,* **248**, 255 (1988).
248) J. F. Smalley, H. O. Finklea, C. E. D. Chidsey, M. R. Linford, S. E. Creager, J. P. Ferraris, K. Chalfant, T. Zawodzinsk, S. W. Feldberg, and M. D. Newton, *J. Am. Chem. Soc.,* **125**, 2004 (2003).
249) A. Yamakata, T. Uchida, J. Kubota, and M. Osawa, *J. Phys. Chem. B,* **110**, 6423 (2006).
250) A. Yamakata and M. Osawa, *Electrochemistry,* **76**, 208 (2008) [in Japanese].
251) T. A. Germer, J. C. Stephenson, E. J. Heilweil, and R. R. Cavanagh, *J. Chem. Phys.,* **98**, 9986 (1993).
252) E. Schweizer, B. N. J. Persson, M. Tushaus, D. Hoge, and A. M. Bradshaw, *Surf. Sci.,* **213**, 49 (1989).
253) K. Kunimatsu, W. G. Golden, H. Seki, and M. R. Philpott, *Langmuir,* **1**, 245 (1985).
254) H. Noguchi, T. Okada, and K. Uosaki, *J. Phys. Chem. B,* **110**, 15055 (2006).
255) Y. R. Shen, *The Principles of Nonlinear Optics*, John Wiley & Sons, Inc., New York, (1984).
256) J. Holman, P. B. Davies, T. Nishida, S. Ye, and D. J. Neivandt, *J. Phys. Chem. B,* **109**, 18723 (2005).
257) T. Nishida, M. Johnson, J. Holman, M. Osawa, P. B. Davies, and S. Ye, *Phys. Rev. Lett.,* **96**, 77402 (2006).
258) A. Wada, K. Domen, and C. Hirose, *Bunkou Kenkyuu,* **47**, 190 (1999) [in Japanese].
259) S. Ye and M. Osawa, *Hyomenkagaku,* **24**, 740 (2003) [in Japanese].
260) S. Ye, *Bunseki*, 500 (2006) [in Japanese].
261) S. Ye, *Bunseki*, 632 (2006) [in Japanese].
262) Q. Du, E. Freysz and Y. R. Shen, *Science,* **264**, 826 (1994).
263) Q. Du, E. Freysz, and Y. R. Shen, *Phys. Rev. Lett.,* **72**, 238 (1994).
264) D. Eisenberg and W. Kauzmann, *The Structure and Properties of Water*, Oxford University Press, London, (1969).
265) *Faraday Discussion 141: Water-From InterFaces to the Bulk*, from p. 1-487 (2009).
266) A. Morita and J. T. Hynes, *J. Phys. Chem. B,* **106**, 673 (2002).
267) S. Ye, H. Noda, T. Nishida, S. Morita, and M. Osawa, *Langmuir,* **20**, 357 (2004).
268) S. Ye, H. Noda, S. Morita, K. Uosaki, and M. Osawa, *Langmuir,* **19**, 2238 (2003).
269) W. Zhou, S. Ye, M. Abe, T. Nishida, K. Uosaki, M. Osawa, and Y. Sasaki, *Chem.-Eur. J.,* **11**, 5040 (2005).
270) Z. Schultz, M. Biggin, J. White, and A. A. Gewirth, *Anal. Chem.,* **76**, 604 (2004).
271) S. Baldelli, N. Markovic, P. Ross, Y. R. Shen, and G. Somorjai, *J. Phys. Chem. B,* **103**, 8920 (1999).
272) F. Dederichs, K. A. Friedrich, and W. Daum, *J. Phys. Chem. B,* **104**, 6626 (2000).
273) G. Q. Lu, A. Lagutchev, D. D. Dlott, and A. Wieckowski, *Surf. Sci.,* **585**, 3 (2005).
274) K. A. Friedrich, W. Daum, F. Dederichs, and W. Akemann, *Z. Phys. Chem.,* **217**, 527 (2003).
275) H. Ohno and K. Fukumoto, *Electrochemistry,* **76**, 16 (2008).